Supported Mono- and Bimetallic Gold Nanoparticle Catalysts for Different Organic Transformations

Sisodiya, Sheetal

2017

Document Version:
Publisher's PDF, also known as Version of record

Supported Mono- and Bimetallic Gold Nanoparticle Catalysts for Different Organic Transformations

CENTRE FOR ANALYSIS AND SYNTHESIS | LUND UNIVERSITY
SHEETAL SISODIYA

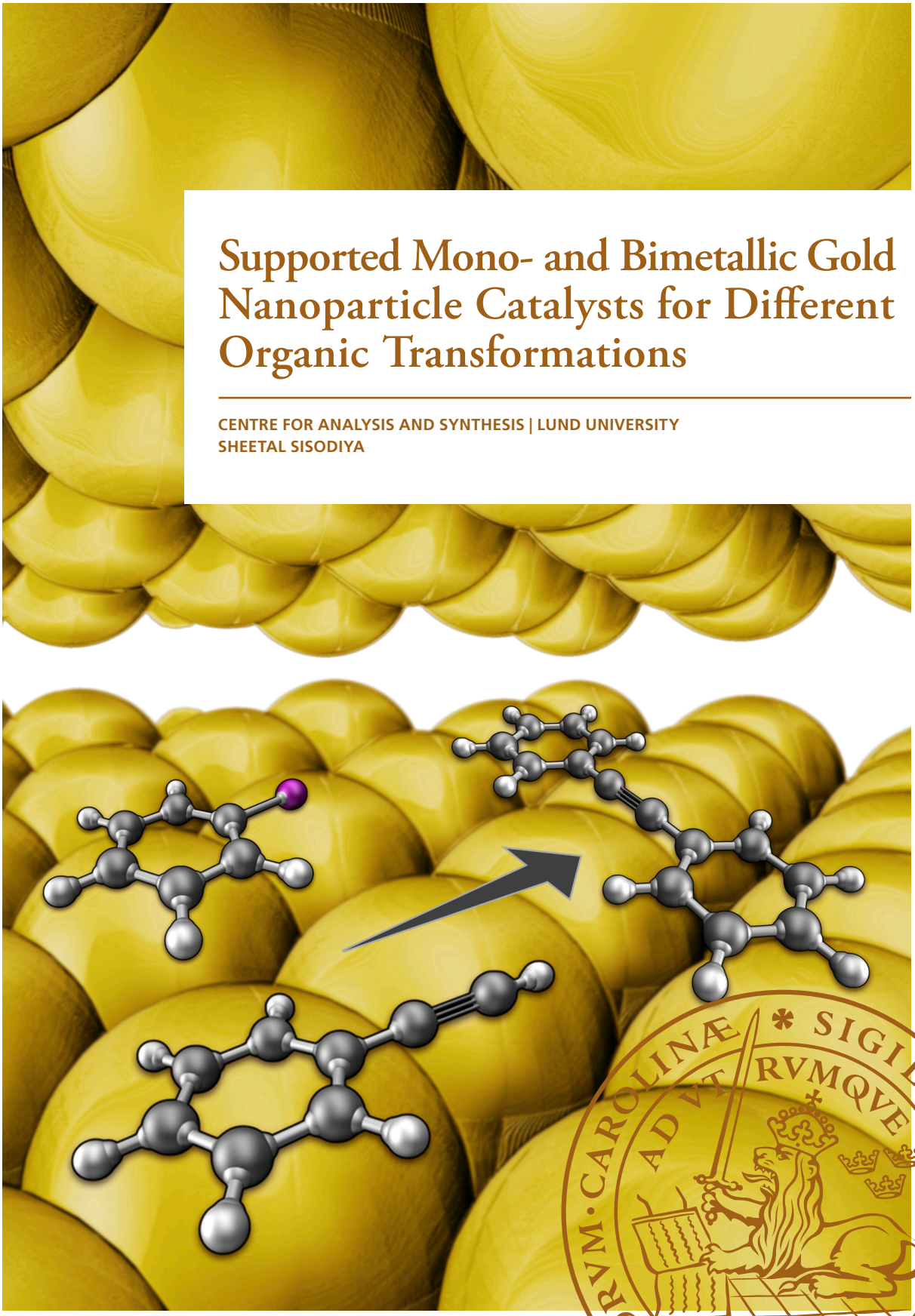

Supported Mono- and Bimetallic Gold Nanoparticle Catalysts for Different Organic Transformations

Sheetal Sisodiya

LUND
UNIVERSITY

DOCTORAL DISSERTATION
To be publicly defended for the degree of PhD at the Faculty of Science, Lund University, Sweden in Lecture Hall F, Kemicentrum, Lund, on Thursday, 15th June, 2017 at 9.15 am.

Faculty opponent
Assoc. Prof. Susanne Mossin, Department of Chemistry,

Technical University of Denmark

Organization	Document name
LUND UNIVERSITY	DOCTORAL DISSERTATION
	Date of issue 2017-05-22
Author: Sheetal Sisodiya	Sponsoring organization

Title

Supported Mono- and Bimetallic Gold Nanoparticle Catalysts for Different Organic Transformations

Abstract:

Supported gold nanoparticles are emerging as an important class of catalysts for various organic transformations due to their tunable properties. This thesis embraces the fundamental studies of supported gold nanoparticles for different organic reactions from the viewpoint of understanding the role of synthesis methods, nature of carriers, and addition of second metal on the properties and functions of gold catalysts. The catalysts are synthesised by different routes, namely: deposition-precipitation, incipient wetness impregnation, and sol-immobilisation, and characterised ex situ by techniques such as X-ray fluorescence, N_2 sorption, powder X-ray diffraction, X-ray photoelectron spectroscopy, and various types of electron microscopy. The reactions investigated include: (i) Sonogashira coupling, which is a unique method for the cross coupling between *sp* and sp^2 or sp^3 carbon atoms; (ii) epoxidation of styrene to styrene oxide; (iii) oxidation of ethylbenzene to acetophenone; and (iv) oxidative cross coupling of non-activated arenes. All these transformations lead to important intermediates which have numerous applications in polymer, perfume and/or pharmaceutical industries. In Sonogashira coupling of phenylacetylene and iodobenzene over Au/CeO_2, Au/TiO_2, and Au/Al_2O_3 catalysts, impact of synthesis routes, nature of support and Au particle size was studied. It is found that the catalysts prepared by deposition-precipitation lead to higher activity than their analogues obtained by incipient impregnation method due to a better dispersion and smaller size (4-15 nm) of gold particles on the former than the latter. In addition, redox (CeO_2, TiO_2) supports are more active than non-redox (Al_2O_3) carrier. Evaluation of gold nanoparticles supported on mesoporous materials (MCM-41, SBA-15, KIT-6 and fumed SiO_2) in styrene epoxidation demonstrates Au/MCM-41 as the best system, due to its smallest Au size (ca. 3 nm), leading to full styrene conversion in 10 h with 96% styrene oxide selectivity. This is the best performance reported for these types of catalysts to date. Still, the attainment of full selectivity was not possible by above systems and thus the bimetallic Au-Pd nanoalloy supported in TiO_2 was investigated in styrene oxidation, which enables full conversion with 99% selectivity to styrene oxide in 12 h due to electronic interactions between Au and Pd. This study marks the first application of Au-Pd in styrene epoxidation. Besides, the Au-Pd/TiO_2 catalyst also shows good activity in ethylbenzene oxidation. Oxidative cross coupling of bromoanisole with benzene is studied over Au/ZrO_2, Au/TiO_2, and Au/Al_2O_3, where the former leads to the best productivity of cross coupled product due to the combination of smaller gold nanoparticles and redox nature of support. Overall, these studies suggest that the attainment of superior performance on supported gold nanoparticle catalysts relies on the appropriate choice of support, catalyst preparation route, and/or addition of second metal that could interact with gold.

Key words Gold nanoparticles, coupling reaction, styrene epoxidation, bimetallic nanoparticle, supported gold nanoparticle

Classification system and/or index terms (if any)

Supplementary bibliographical information		Language: English
ISSN and key title		ISBN 978-91-7422-533-4 (Print) ISBN 978-91-7422-534-1 (Pdf)
Recipient's notes	Number of pages 156	Price
	Security classification	

Signature  Date 2017-05-08

Supported Mono- and Bimetallic Gold Nanoparticle Catalysts for Different Organic Transformations

Sheetal Sisodiya

LUND
UNIVERSITY

Cover photo designed by Roman Gritcenko

Faculty of Science
Department of Chemistry
Centre for Analysis and Synthesis

ISBN 978-91-7422-533-4 (Print)
ISBN 978-91-7422-534-1 (Pdf)

Printed in Sweden by Media-Tryck, Lund University
Lund 2016

Media-Tryck is an environmentally certified and ISO 14001 certified provider of printed material. Read more about our environmental work at www.mediatryck.lu.se

कर्मण्येवाधिकारस्ते मा फलेषु कदाचन।

मा कर्मफलहेतुर्भूर्मा ते सङ्गोऽस्त्वकर्मणि॥ २-४७

(Bhagwat Gita: Chapter Two verse 47)

You have a right to perform your prescribed duty, but you are not entitled to the fruits of action. Never consider yourself the cause of the results of your activities, and never be attached to not doing your duty.

Dedicated to my parents and my husband

Content

Popular Science Summary

"Catalysis" is a field of science that relates to the increase of the rate of a chemical reaction through the involvement of an additional substance, known as "catalyst", which acts without being consumed. Among all known types, heterogeneous catalysis, where the catalyst is in different phase than the reactants, plays a pivotal role in the sustainable development of the modern society with its dominance through catalysing more than 80% of industrial chemical processes.

Recently, "supported gold nanoparticles", inorganic composite materials in which nano-sized gold particles are carried on solid carriers such as metal oxides, have emerged as an important class of catalysts enabling to attain superior selectivities and yields of the desired products compared to previously known systems. One of the key features of gold catalysts involve its adaptable properties, tuned through the application of modern synthesis tools, carriers of different natures, and/or combining gold with other metals, making them suitable to catalyse a number of important organic reactions.

In this thesis, supported gold nanoparticle catalysts are investigated for organic reactions, viz. Sonogashira cross coupling, styrene oxidation, ethylbenzene oxidation, and oxidative cross coupling, which are useful in pharmaceutical, perfume, polymer, and cosmetics industries. Through the precision synthesis, advanced characterisation, and catalytic evaluations, synthesis-structure-activity relationships are established, which helped to develop a fundamental understanding of gold catalysis in these reactions and enabled to design superior gold-based catalysts leading to better performance than those reported previously.

Acknowledgement

First and foremost I would like to thank my PhD supervisor Prof. Ola F. Wendt for giving me this unique opportunity to work in his research group and allowing me to work independently. I thank my co-supervisor Prof. Joachim Schnadt for helping me during my beam times.

My appreciation also extends to the present and past group members, Katya for your positive thoughts, Maitham for helping me whenever needed, Mike, Sasha, Abdelrazek, Solomon, Rachael, Alexy, Magnus, Klara, Kevin, Roman, Sudarkodi, and Nagarajan. (Naga) I am so grateful to have you as my colleague because during my starting days when I was completely new to Sweden you were the one who introduced me to Swedish system.

The work in this thesis has also benefited from a number of collaborations and I would like to take this opportunity to thank all the collaborators. Prof. Leif Johansson is sincerely thanked for doing XRF of my samples without delaying anytime. Likewise, Prof. Reine Wallenberg and Axel are acknowledged for TEM. Dr. Erik Lewin for XPS. Shilpi, Niclas, Payam, and Ben for helping me in my beamtimes and data analysis. I am also thankful to my former lab mates from NCL, India, Anish and Pandiraj for doing TEM.

I thank Abdoh Ismail and late Clas Wesen for all help and technical advice regarding gas chromatography. I also thank Carola for helping me with powder X-ray diffraction machine.

I acknowledge Maria, Bodil, and Katarina for your help with administrative work and ordering of chemicals.

I would like to express my appreciation to my friends in Lund, Tripta for always cheering me up and I cannot forget summer time or excursions, which I did with you. Priya, for taking care of me during my life's most critical moment and always fulfilling my wishes regarding any Indian food item. I also thank Gunjan, Prashant, Partha, and Santanu.

I take this occasion to thank all my teachers, well-wishers, classmates & friends in various stages for their love, encouragement and kind cooperation that I received from them whose names are not mentioned here. I would like to thank all the people from CAS.

Above ground, I am indebted to my mother Nirja Sisodiya, father K. R. Sisodiya for making me capable to stand on the place where I am today and your value to me grows with age. To my elder sister Mamta Shende for your constant positive criticism and always giving me positive hope (Geeta updesh) during my low times. Lots of love to my nephew Ayan Shende. I am also thankful to my brother Anand Sisodiya and brother in-law Abhay Shende. Words cannot explain how grateful I am to have wonderful in-laws.

Last but not least I cannot express my gratitude in words to my beloved, understanding, and supportive husband Amol Amrute, without your constant support and love I cannot imagine my life. Because of you I am able to finish my PhD without being stressed up so much. And finally, my love goes to my little princess/gem Maneeka who has completed my life.

Abbreviations

NP	Nanoparticles
Au NPs	Gold nanoparticles
MCM-41	Mobile Composition of Matter no.41
SBA-15	Santa Barbara Amorphous
PXRD	Powder X-ray diffraction
XRD	X-ray diffraction
TEM	Transmission electron microscopy
HAADF	High angle annular dark field
STEM	Scanning transmission electron microscopy
XPS	X-ray photoelectron spectroscopy
XAS	X-ray absorption spectroscopy
XRF	X-ray fluorescence
XEDS	X-ray energy dispersive spectroscopy
EDXRF	Energy dispersive X-ray fluorescence
WDXRF	Wavelength dispersive X-ray fluorescence
BET	Brunauer-Emmett-Teller
BJH	Barrett-Joyner-Halenda
ICDD	International Center for Diffraction Data
LBA	Line broadening analysis
FWHM	Full width at half maximum
NHC	N-heterocyclic carbenes
Dp	Diffraction pattern
PA	Phenylacetylene

IB	Iodobenzene
DPA	Diphenylacetylene
BP	Biphenyl
DPDA	Diphenyldiacetylene
DP	Deposition-precipitation
IMP	Impregnation
PVA	Polyvinyl alcohol
SO	Styrene oxide
BZ	Benzaldehyde
ACP	Acetophenone
DMF	*N,N*-Dimethylformamide
ACE	Acetonitrile
TBHP	*tert*-Butyl hydroperoxide
H_2O_2	Hydrogen peroxide
EB	Ethylbenzene
MOF	Metal Organic Framework
$PhI(OAc)_2$	(Diacetoxyiodo)benzene

List of Publications

The thesis is comprised of papers, which are shown below:

Paper I

Sonogashira coupling reaction over supported gold nanoparticles: Influence of support and catalyst synthesis route

Sheetal Sisodiya, L. Reine Wallenberg, Erik Lewin, Ola F. Wendt, *Appl. Catal. A: Gen., **2015**, 503, 69.*

Paper II

On the effects of co-dosing phenylacetylene with halogenated benzene on Au(111) surface

Niclas Johansson, Sheetal Sisodiya, Shilpi Choudhary, Jesper. N. Andersen, Jan Knudsen, Ola F. Wendt, Joachim Schnadt, in manuscript form

Paper III

Selective styrene epoxidation over gold nanoparticles supported on mesoporous material

Sheetal Sisodiya, Ola F. Wendt, submitted

Paper IV

Oxidative cross-coupling of non-activated arenes catalysed by supported gold nanoparticles

Sheetal Sisodiya, Erik Lewin, Ola F. Wendt, in manuscript form

Paper V

TiO_2 supported Au-Pd nanoalloy catalyst for styrene oxidation with very high selectivity

Sheetal Sisodiya, Axel R. Persson, L. Reine Wallenberg, Erik Lewin, Ola F. Wendt, submitted

My Contribution to the Papers

Paper I

I have performed the synthesis of catalyst and its catalytic activity, for characterisation I have participated in TEM measurements, PXRD is done by me and other characterisation is done by collaborators but analysis was done by me. I wrote the full manuscript.

Paper II

I have conceived the project plan. Participated in X-ray photoelectron and absorption spectroscopy measurements.

Paper III

I have conceptualised the project and performed all the experiments. I have participated in TEM measurements. I did PXRD and XRF. I wrote the full manuscript.

Paper IV

I have conceptualised the project and performed all the synthesis, catalytic activity, I have participated in TEM measurements and XRF, PXRD was done by me. Collaborators did other characterisation. I wrote the full manuscript.

Paper V

I have designed and performed all the experiments. After initial experiments I synthesised catalyst. I did PXRD, XRF. Further, I have participated in TEM sessions. My collaborators did other characterisation. I wrote the full manuscript.

General Introduction

Background

Human beings have recognised the existence of gold for about 7000 years. Gold is one of the metal, which is naturally present in the metallic form. Pure gold is a soft metal and due to its softness it can be used in making jewellery, coins, and decorative objects. For more than a century, bulk gold was considered to be a catalytically inert material. The only known chemistry of gold was associated with the wine red colour of colloids in stained glass windows of cathedrals and churches. One of the earliest attempts to prepare very small gold particles was by Michael Faraday in 1857.[1] He prepared ''finely divided'' gold particles and nearly a century later by electron microscopy characterisation it was found that these particles are ''nanoparticles'' having size in the range of 6±2 nm.[1] Later it was found that, when gold is present in nanometre scale (i.e gold nanoparticles) it leads to the highly effective catalyst, generating a popular research topic in the frontier between homogeneous and heterogeneous catalysis.[2,3] In this respect, the pioneering work by Haruta et al.[4] on CO oxidation with gold nanoparticles (he entitled them 'gold crystallites') supported on base metal oxides and by Hutchings et al.[5,6] on hydrochlorination of ethylene with gold chloride supported on activated carbon paved the way for discovering important catalytic applications of gold nanoparticles. The latter included studies of supported gold nanoparticles in organic transformations such as the aerobic oxidation of methanol to methyl formate, the bulk production of vinyl acetate, hydroamination of olefin, oxidation of olefins, C-C coupling, silane oxidation, alkyne activation, reduction via transfer hydrogenation, and basic raw chemicals for the synthesis of polymers.[7-15]

In gold catalysis two aspects play a crucial role in controlling catalyst activity and selectivity, namely: (i) the nature of the gold species and (ii) the size of the gold nanoparticles. For instance Wu et al. reported Au(0) as the active species in cyclohexane oxidation,[16] while Corma et al. reported Au(I) as the active species in the Sonogashira coupling.[17] Thus, for some reactions Au(0) is the active species, while others are catalysed by ionic gold. With regard to the particle size it is

believed that the smaller the particle size the better is the performance. These key features of supported gold catalyst can be tuned by the nature of the support as well as by the applied preparation route. Besides, an appropriate support plays a key role in stabilising the formed nanoparticles by reducing their mobility due to strong interactions and thus, suppressing agglomeration or sintering of gold nanoparticles. Moreover, redox active supports, such as TiO_2, CeO_2, Fe_3O_4, and MnO_2 could participate in the reaction mechanism by redox cycling.[18] Among different known supports, metal oxides e.g. TiO_2, CeO_2, Fe_3O_4, MgO, etc. are the most widely used. The catalytic activity of gold is directly related to the particle size in the nanometre length scale and it vanishes completely as the particle size grows into the micrometric scale. Therefore, for the attainment of smaller Au particles different synthesis methods have been used, for instance impregnation, co-precipitation, deposition precipitation, deposition-reduction, and sol-immobilization.[19-25]

Apart from the nature of gold species, the type of support, and the size of the gold nanoparticles the fourth factor that can play a crucial role in controlling activity and selectivity is alloying of gold with different metals. In this regard, bimetallic and trimetallic gold-bearing nanoalloys[26, 27] are being heavily studied. It has been observed that the properties of bimetallic catalysts are different from their monometallic analogues because of ‘‘synergistic’’ effects between the two metals. Due to this effect it is possible to achieve high selectivity for desired product. There are different methods used in synthesis of bimetallic catalyst such as

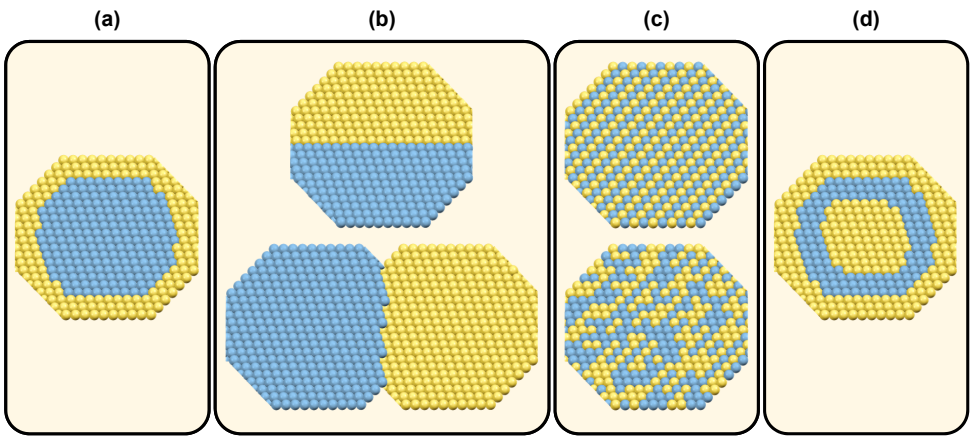

Figure. 1 Some possible mixing patterns in bimetallic systems: (a) core–shell alloys, (b) sub-cluster segregated alloys, (c) ordered and random homogeneous alloys, and (d) multishell alloys. Figure modified from ref 29.

chemical reduction, thermal decomposition of appropriate precursors, electrochemical synthesis, radiolysis, sonochemical synthesis, and template synthesis. Among these methods, the chemical reduction method can be further sub-classified into (i) co-reduction, (ii) reduction of bimetallic metal complexes and (iii) successive reduction.[28] Ferrando et al. have reported four possible types of mixing patterns between the two metals, which are shown in **Figure 1**.[29] Among these the most commonly observed mixing is core shell (a) and random nanoalloys (c). The relative strength of the bond, the surface energy, and relative atomic sizes between the two metals decide the type of mixing pattern that will be obtained.

Thus, understanding the science of supported gold nanoparticle catalyst through in depth study of the impact of synthesis route, nature of support, and alloying of gold with a second metal is highly relevant to design suitable catalysts, attaining the best performance in important organic transformations for example, Sonogashira coupling of phenylacetylene and iodobenzene, oxidative cross coupling of non-activated arenes, and oxidation of styrene and ethylbenzene.

Aim of the thesis

The principal aim of this thesis was to develop suitable monometallic and bimetallic Au NP catalysts supported on metal oxides and mesoporous materials to achieve better activity and selectivity in coupling and oxidation reactions. To accomplish this aim different catalyst synthesis method and different supports were studied. Catalysts were characterised using a battery of techniques viz. XRF, PXRD, N_2 sorption, TEM, EDX, and XPS and catalytic testing in either coupling or in oxidation reaction was performed.

Outline of the thesis

The thesis contains five chapters. **Chapter 1** gives a description about the synthesis method and characterisation techniques used in this work. The lack of a comparative study of different supports and synthesis method for Au NPs supported on metal oxides (Au/CeO_2, Au/TiO_2, and Au/Al_2O_3) in Sonogashira coupling, encouraged us to shed light on this issue and the obtained results are presented in **Chapter 2**. In addition, the study of gas phase Sonogashira coupling

on Au(111) surface unravel the key aspect of the mechanism involved in Sonogashira coupling reaction and the results are included in **Chapter 2** .

Chapter 3 describes the synthesis, characterisation of Au NPs supported on mesoporous materials (MCM-41, SBA-15, KIT-6, SiO_2). All the synthesised catalyst were used in styrene epoxidation using TBHP as an oxidant. The best catalyst system has been used in optimising reaction parameters.

Chapter 4 investigates the use of Au/ZrO_2 as a catalyst in the oxidative coupling of Br-anisole and benzene. It starts with the synthesis of Au/ZrO_2 catalyst and its characterisation by XRF, PXRD, N_2 sorption, TEM, and XPS. The results from the oxidative coupling reaction shows that the catalyst is selective for the desired heterocoupling product over the homocoupling product.

The application of bimetallic Au-Pd supported on TiO_2 as a catalyst in styrene and ethylbenzene oxidation is presented in **Chapter 5**, followed by the comparison of bimetallic $Au\text{-}Pd/TiO_2$, with the monometallic counterparts. The best catalyst i.e $Au\text{-}Pd/TiO_2$ was used in optimisation of styrene epoxidation reaction parameters.

Each chapter in this thesis was written based on one or more separate publications and can be read independently. Accordingly, some overlap cannot be avoided

References

1. M. Faraday, *Philos. Trans. R. Soc.* London, **1857**, 147, 145; J. Turkevich, P. C. Stevenson, J. Hillier, *Discuss. Faraday Soc.*, **1951**, 11, 55.
2. D. Astruc, F. Lu, J. Aranzaes, *Angew. Chem., Int. Ed.*, **2005**, 44, 7852.
3. M. Daniel, D. Astruc, *Chem. Rev.*, **2004**, 104, 293.
4. M. Haruta, N. Yamada, T. Kobayashi, S. Iijima, *J. Catal.*, **1989**, 115, 301.
5. G. Hutchings, *J. Catal.*, **1985**, 96, 292.
6. B. Nkosi, J. Coville, G. Hutchings, *Appl. Catal. A Gen.*, **1988**, 43, 33.
7. C. Christensen, J. Norskov, *Science*, **2010**, 327, 278.
8. T. Ishida, M. Haruta, *Angew. Chem., Int. Ed.*, **2007**, 46, 7154.
9. A. Wittstock, V. Zielasek, J. Biener, C. Friend, M. Baumer, *Science*, **2010**, 327, 319.
10. R. Meyer, S. Shaikhutdinov, H. Freund, *Gold Bull.*, **2004**, 37, 72.
11. N. Patil, *ChemCatChem*, **2011**, 3, 1121.
12. P. Lignier, F. Morfin, L. Piccolo, J. Rousset, V. Caps, *Catal. Today*, **2007**, 122, 284.
13. S. Sisodiya, L. R. Wallenberg, E. Lewin, O. F. Wendt, *Appl. Catal. A Gen.*, **2015**, 503, 69.
14. A. Caporusso, L. Aronica, E. Schiavi, G. Martra, G. Vitulli, P. Salvadori, *Organomet. Chem.*, **2005**, 690, 1063.
15. F. Su, L. He, J. Ni, Y. Cao, H. He, K. Fan, *Chem. Commun.*, **2008**, 3531.
16. P. Wu, Z. Xiong, K. P. Loh, X. S. Zhao, *Catal. Sci. Technol.*, **2011**, 1, 285.
17. C. Gonzalez-Arellano, A. Abad, A. Corma, H. Garcia, M. Iglesias and F. Sanchez, *Angew. Chem., Int. Ed.*, **2007**, 46, 1536.
18. M. Haruta, *Catal. Today*, **1997**, 36, 153.
19. A. Corma, H. Garcia, *Chem. Soc. Rev.*, **2008**, 37, 2096.
20. Z. Ma, S. Dai, *ACS Catal.*, **2011**, 1, 805.
21. R. Bonelli, C. Lucarelli, T. Pasini, L. Liotta, S. Zacchini, S. Albonetti, *Appl. Catal. A Gen.*, **2011**, 400, 54.
22. M. Haruta, T. Kobayashi, H. Sano, N. Yamada, *Chem. Lett.*, **1987**, 16, 405.

23. S. Tsubota, D. Cunningham, Y. Bando, M. Haruta, *Stud. Surf. Sci. Catal.*, **1995**, 91, 227.
24. T. Ishida, S. Okamoto, R. Makiyama, M. Haruta, *Appl. Catal. A Gen.*, **2009**, 353, 243.
25. L. Prati, G. Martra, *Gold Bull.*, **1999**, 32, 96.
26. C. Bracey, R. Ellis, G. Hutchings, *Chem. Soc. Rev.*, **2009**, 38, 2231.
27. J. Gong, *Chem. Rev.*, **2012**, 112, 2987.
28. M. Sankar, N. Dimitratos, P. Miedziak, P. Wells, C. Kielye, G. Hutchings, *Chem. Soc. Rev.*, **2012**, 41, 8099.
29. R. Ferrando, J. Jellinek and R. L. Johnston, *Chem. Rev.*, **2008**, 108, 845.

Chapter 1. Catalyst Synthesis and Characterisation Techniques

1.1 Catalyst synthesis

In this thesis three synthesis methods are used to synthesise the catalyst, namely: deposition-precipitation (DP), incipient wetness impregnation (IMP), and sol-immobilisation.

Deposition-precipitation (DP)

In the deposition-precipitation route (**Scheme 1.1**), an aqueous solution of gold salt was prepared and the pH of the solution was brought to 7 using a 1 M NaOH solution. Once the pH was stable the carrier oxide was added to the aqueous solution of gold salt and stirred for 3 h at 80°C, followed by filtration and thorough washing with water until no traces of Cl^- ions were detected by the $AgNO_3$ test. This is an important treatment since traces of Cl^- that remain strongly bonded to gold are highly detrimental for the overall activity. The obtained solid was dried at 60°C for 12 h and calcined in static air at 400°C for 5 h.

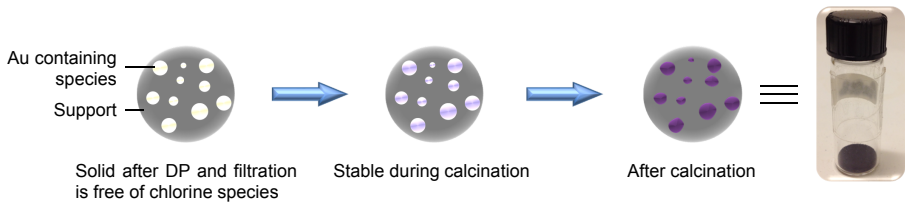

Scheme 1.1 Schematic showing the DP synthesis route.

Incipient wetness impregnation

In the incipient wetness impregnation method, the carrier metal oxide powder was added to the aq. gold salt solution and stirred to obtain a homogeneous just-wet solid. The latter was dried at 60°C for 12 h and calcined at 400°C for 5 h in static air. This method gives bigger gold particles because of agglomeration, which is

caused by chlorine species present in the gold salt and are not removed by washing unlike, in the DP method where all the chlorine species are remove by washing. These chlorine species deposit on the carrier during preparation and induces the migration of gold species during calcination generating larger gold agglomerates (**Scheme 1.2**).[1]

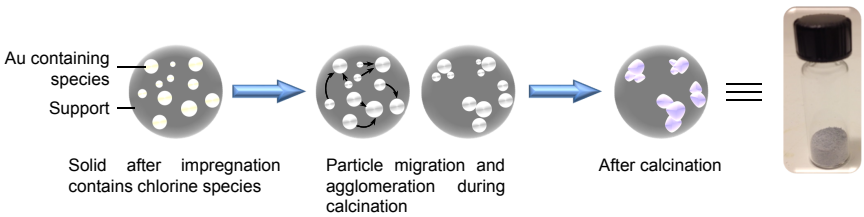

Scheme 1.2 Proposed schematic showing role of chlorine on the formation/agglomeration of gold nanoparticles on the solid support.

Sol-immobilisation

To a required amount of polyvinyl alcohol (PVA) solution an aqueous solution of metal (of the desired concentration) was added, after stirring for 10 min a freshly prepared solution of 0.1 M $NaBH_4$ was added. After 30 min of stirring, the support was added to this solution under vigorous stirring and continued stirring for 20 h. The obtained slurry was filtered and washed with copious amount of distilled water. The obtained solid was dried at 120°C for 16 h and calcined at 400°C for 2 h.

1.2 Characterisation techniques

Different characterisation techniques were used to know the properties of the synthesised materials. Primarily Powder X-ray diffraction (PXRD), N_2 sorption, and XRF were used. After optimisation, the best catalyst was further characterised by TEM and XPS. PXRD was used to obtain information about the phase of the metal and particle size. Metal content was analysed by XRF. The specific surface area of the catalyst is of interest and it is acquired by N_2 adsorption/desorption measurements. TEM was mainly used for calculation of particle size and lattice fringe distance was calculated to confirm the presence of gold particles, and chemical composition of the catalyst was gained by X-ray energy dispersive spectroscopy (EDX). The oxidation state of the metal was evaluated by an

invaluable tool i.e XPS. All of these acquired data are of importance to understand the properties of the synthesised catalysts.

1.2.1 X-ray Fluorescence (XRF)

Introduction

X-ray fluorescence (XRF) spectrometry is an analytical technique used for elemental analysis of solids, liquids, and thin-film samples. Both major and trace (ppm-level) components can be analysed. The analysis is rapid and usually sample preparation is minimal or not required at all. Henry Moseley was perhaps the father of this technique. However, until 1940's the techniques was not practical and in 1950's the first commercial X-ray spectrometers were produced. [2-5]

Theory

When a high-energy electron beam interacts with matter two things happen which are shown in **Figure 1.1**: (i) emission of photoelectron and (ii) ejection of photoelectrons from the inner shells of the atoms leaves a "hole" in the electronic structure of the atom, and an electron from a higher energy shell fills the hole. During this the atom undergoes fluorescence, or the emission of an X-ray photon whose energy is equal to the difference in energies of the initial and final states. Detecting this photon and measuring its energy allows determining the element and specific electronic transition from which it originated. [6,7]

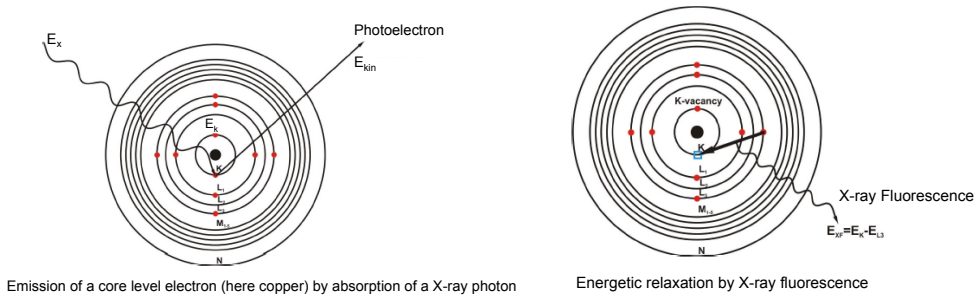

Emission of a core level electron (here copper) by absorption of a X-ray photon

Energetic relaxation by X-ray fluorescence

Figure 1.1 Interaction of electron beam with matter.

Instrumentation

There are two types of XRF instruments: wavelength dispersive (WD) and energy dispersive (ED) spectrometer. Their schematic representation is shown in **Figure 1.2 and 1.3**. Further, these two spectrometer differs in detection system. EDXRF systems depend on semiconductor-type detectors. WDXRF spectrometers, however, use an analysing crystal to disperse the emitted photons based on their wavelength and place the detector in the correct physical location to receive X-rays of a given energy. Instrument which has used for the present work is a Thermo Scientific Niton XL3t XRF Analyser GOLDD+ instrument with a Ag anode and is EDXRF.

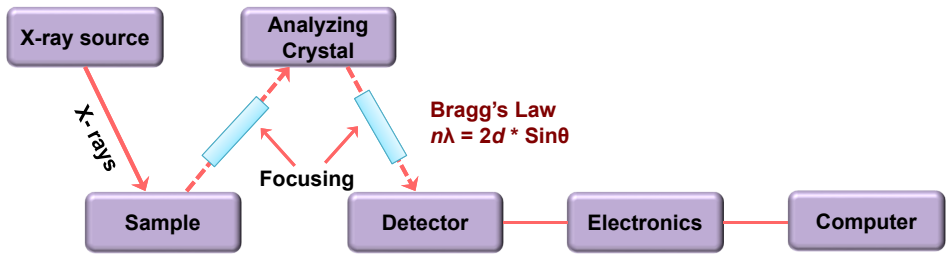

Figure 1.2 Schematic represenation of wavelength dispersive XRF (WDXRF).

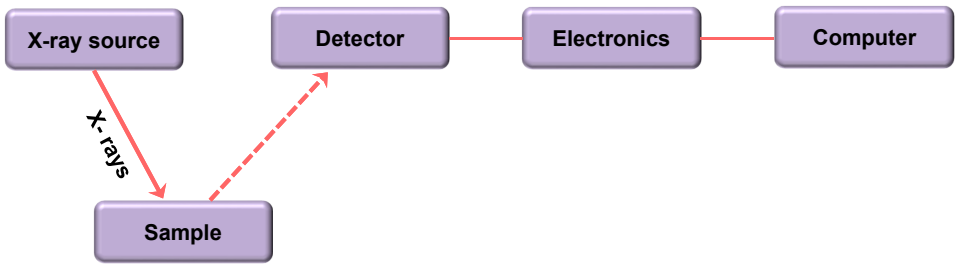

Figure 1.3 Schematic represenation of energy dispersive XRF (EDXRF).

1.2.2 Nitrogen adsorption-desorption

Introduction

There are two important physical properties; surface area and porosity which determines the quality and utility of solid catalyst. It also determines how much bulk material is accessible to reactant molecules. It is observed that most of the catalysts which are highly porous and possess large specific surface areas are

active. But this catalytic activity may be only indirectly related to this "total" surface, still the determination of surface area is generally considered to be an important requirement in catalyst characterisation[8]. In addition, information about pore structure is usually necessary since this may control the transport of the reactants and products of a catalytic reaction.

Theory

Gas adsorption methods are most often used to determine the surface area and pore size distribution of catalysts. In most of the measurements nitrogen is used as adsorption gas and to calculate surface area, pore volumes, and pore size distributions of porous solids from N_2 physisorption isotherm data, Brunauer-Emmett-Teller (BET) method is used. The BET equation can be represented as:

$p/V(p_o\text{-}p) = 1/cV_m + [(c\text{-}1)/cV_m]\ (p/p_o)$

where, p is adsorption equilibrium pressure,

p_o is saturation vapour pressure of the adsorbate at the experimental temperature,

V is volume of N_2 adsorbed at pressure p,

V_m is volume of adsorbate required for monolayer coverage

and c is a constant that is related to the heat of adsorption and liquefaction.

A linear relationship between $p/V(p_o\text{-}p)$ and p/p_o is required to obtain the quantity of nitrogen adsorbed.

The monolayer volume, V_m is given by $1/(S+I)$

where S is the slope and is equal to $(c\text{-}1)/cV_m$ and

I is the intercept equal to $1/cV_m$.

The surface area of the catalyst (S_{BET}) is related to V_m, by the equation, $S_{BET} = (V_m/22414)\ N_a\sigma$, where N_a is Avogadro number and σ is mean cross sectional area covered by one adsorbate molecule. The σ value generally accepted for N_2 is 0.162 nm^2.

Six types of physisorption isotherms are found which are shown in **Figure 1.4**.[9] Type I to V classified by Brunauer, Denning, and Teller and type VI by Adamson.

Type I isotherms are given by microporous catalysts such as molecular sieve zeolites and many activated carbon supports.

Type II isotherms shows monolayer-multilayer adsorption on a heterogeneous non-porous substrate.

Type III and V are rare in that adsorbate interactions are weak, typical for vapours.

Type IV is for system showing the presence of narrow pores. The ''hysteresis loop'' is characteristic of type IV system and is result of capillary condensation.

Type VI is readily obtained with nobel gas adsorption on well-defined uniform solids.

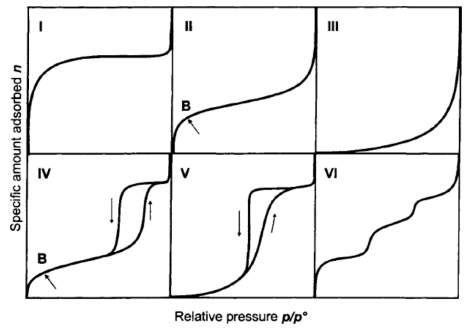

Figure 1.4 Six types of gas physisorption isotherms.

Several computational procedures are available for the derivation of pore size distribution of samples from physisorption isotherms. Most popular among them is the Barrett-Joyner-Halenda (BJH) model, which was introduced in 1951. This is a procedure for calculating pore size distributions from experimental isotherms using the Kelvin model of pore filling. It applies only to the mesopore and small macropore size range. The mesopores size distribution is usually expressed as a plot of $\Delta V_p/\Delta r_p$ versus r_p, where V_p = mesopore volume, and r_p = pore radius. It is assumed that the mesopores volume is completely filled at high p/p_0.

Instrumentation

The BET surface area of samples was measured under liquid N_2 temperature, using N_2 as an adsorbent. In this thesis the N_2 sorption was measured using a Micromeritics ASAP 2400 V3.06 instrument, where all samples were de-gassed at 423 K for 24 h prior to the analysis. The isotherms were analysed in a conventional manner in the region of the relative pressure, p/p_0 = 0.05 to 0.3. The BJH method was used to determine the area of the pore walls and uses the Kelvin equation to correlate the partial pressure of nitrogen in equilibrium with the porous solid to the size of the pores where capillary condensation takes place. The pore size distribution is obtained by analysis of the desorption isotherm. [10,11]

1.2.3 Powder X-ray Diffraction (PXRD)

Introduction

In heterogeneous catalysis the active sites are usually located on the solid surface, but the bulk structure plays an important role, because many of the catalyst characteristics depend on it. X-ray diffraction is main technique to investigate the bulk structure of catalyst. Till the end of 1970s, single crystal X-ray diffraction has been mainly used for structure analysis. However, from 1990s it is possible to use powder X-ray diffraction (PXRD) for structure analysis. This evolution has solved the problem of analysing heterogeneous catalyst because in most cases it is hard to grow crystal of the catalyst used in reaction.[12]

Theory

The XRD method involves the interaction between the incident monochromatized X-rays (like Cu K_α or Mo K_α source) with the atoms of a periodic lattice. X-rays scattered by atoms in an ordered lattice interfere constructively in directions given by Bragg's law: $n\lambda = 2d \sin\theta$, where, λ is the wavelength of the X-rays, d is the distance between two lattice planes, θ is the angle between the incoming X-rays and the normal to the reflecting lattice plane and n is an integer known as the order of reflection.[13] PXRD can be used for identification of phase. The identification of phase is based on the comparison of the set of reflections of the sample with that of pure reference phases distributed by International Center for Diffraction Data (ICDD).

For Characterisation of supported metal crystallites X-Ray diffraction line broadening analysis (LBA) has been widely used. Line broadening analysis can be carried out, either at an elementary level, or a more sophisticated level. At the simplest level, the application of the Scherrer formula leads to an estimate of the mean crystallite size.

Debye-Scherrer formula: $D_{hkl} = k\lambda/\beta\cos\theta$

where D_{hkl}, is the volume averaged particle diameter

λ is X-ray wavelength

β is full width at half maximum (FWHM)

θ is diffraction angle, respectively,

and k is a constant, often taken as 1.

Instrumentation

The XRD pattern of a powdered sample is measured with a stationary X-ray source (usually Cu Kα) and a movable detector, which scans the intensity of the diffracted radiation as a function of the angle 2θ between the incoming and the diffracted beams. The schematic diagram of a diffractometer system is shown in **Figure 1.5**. When working with powdered samples, an image of diffraction lines occurs because a small fraction of the powder particles will be oriented such that by chance a certain plane (hkl) is at the right angle with the incident beam of constructive interference. Synthesised catalysts were characterised by Powder X-ray diffraction (PXRD) patterns, which were recorded on a STOE & CIE GmbH diffractometer using Cu K_α radiation and Bragg-Brentano geometry with a curved Ge-monochromator. Samples were scanned in a 2θ range of 10-100°.

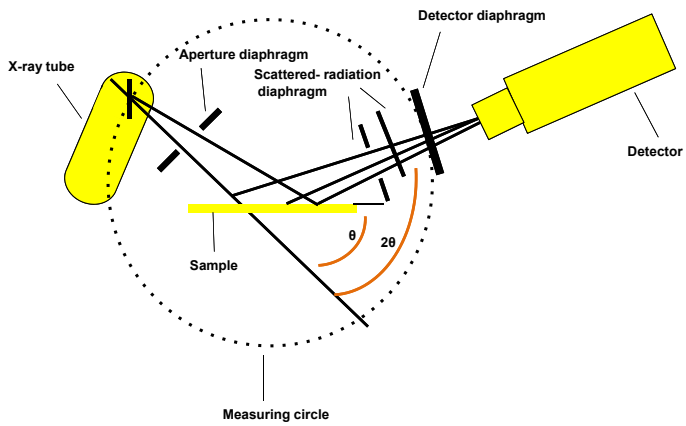

Figure 1.5 Schematic diagram of diffractometer system.

1.2.4 Transmission Electron Microscopy (TEM)

Introduction

Transmission electron microscopy is typically used for high resolution imaging of thin films of a solid sample for micro structural and compositional analysis. Particle size is also calculated from TEM images. TEM is similar to an optical microscope. Most of the TEMs are constructed in the same way regardless of the manufacturer. The first TEM was built by Max Knoll and Ernst Ruska in 1931, and the first commercial TEM was built in 1939. In 1986, Ruska was awarded the Nobel Prize in physics for the development of transmission electron microscopy.

Theory

The TEM involves: (i) irradiation of a very thin sample by a high-energy electron beam, which is diffracted by the lattices of a crystalline or semi crystalline material and propagated along different directions, (ii) imaging and angular distribution analysis of the forward scattered electrons (unlike SEM where backscattered electrons are detected) and (iii) energy analysis of the emitted X-rays.[14] In detail, a primary electron beam of high energy and high intensity passes through a condenser to produce parallel rays, which impinge on the sample. The transmitted electrons form a two-dimensional projection of the sample mass, which is subsequently magnified by the electron optics to produce the so-called bright field image. The contrast in bright field image will depend upon the intensity scattered by the particle and the most contrasted images will be obtained on thin supports with light atoms. Second type of image is dark field image, which is obtained by centering the objective aperture on a diffracted beam, thus excluding the unscattered beam. Then, the image of the particle is bright against a dark background. In dark field image only those particles oriented to give the selected diffracted beam will be imaged.[15-22]

Instrumentation

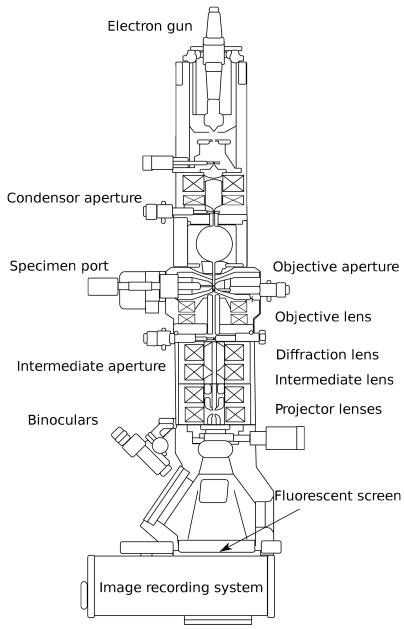

Figure 1.6 Optical components in basic TEM (image taken from wikipedia).

It is easy to understand when the instrument is divided into three components: the illuminating system, the objective lens, and the imaging system. The illuminating system comprises the gun and the condenser lenses. It can be operated in two modes: parallel beam and convergent beam. **Figure 1.6** shows the optical components in TEM. The objective lens and the specimen holder is the main component of TEM. Here the beam-specimen interaction takes place which creates various images and DPs. The imaging system uses several lenses to magnify the image or Dp produced by objective lens and to focus these on the viewing screen or computer display via a detector, CCD, or TV camera.

1.2.5 X-ray Absorption Spectroscopy (XAS)

Introduction

To determine the unoccupied orbital structure of a molecular material as well as its geometric orientation e.g. with respect to a surface XAS is a widely used method. XAS measurements can be performed with samples that are in the gas phase, liquid, and solids. However, one has to consider the fact that interpreting/analysing the XAS data is complicated.

Theory

In XAS, the absorption of X-rays causes the excitation of electrons from a low-energy orbital (a core level) to an unoccupied orbital or into the vacuum. This implies that the energy of the unoccupied orbitals of a compound can be measured by XAS by varying the photon energy and measuring the intensity of the absorption. Moreover, the intensity of the absorption depends on the relative orientation of the X-rays' electric field vector (i.e. the polarisation, which in synchrotron experiments typically is linear) with respect to the orientation of the unoccupied orbitals, and by varying the angle of this electric field vector one can determine the orientation of a molecule in a material.

A typical absorption spectrum shows three regions: The pre-edge region below the absorption edge, the region near to the absorption edge and the region above absorption edge. The region near to the absorption edge is called the near-edge X-ray absorption fine structure (NEXAFS) region and that above the absorption edge is called the Extended X-ray absorption fine structure (EXAFS) region. In this thesis NEXAFS Spectroscopy is used.

Here, the NEXAFS spectrum was measured in electron yield. The absorption event generates a hole in the core level. The hole in core level will eventually be filled either in a fluorescence process or an Auger processes.[23] Since the decay necessarily takes place, measuring the photon energy-dependent intensity of either process implies a measurement of the XAS spectrum. When this is done by measurement of the Auger electron, one says that the spectrum is measured in electron yield.

Instrumentation

In the present study all the X-ray absorption spectra were recorded at beamline D1011 of the MAX II ring of the Swedish national synchrotron radiation facility MAX IV Laboratory in Lund.[24,25] In our experiments we have measured the C Kedge in electron yield. This is very effect, since the yield of Auger electron is much higher as compared to the fluorescence yield for low-Z atoms. Here, use was made of a partial yield detector.

1.2.6 X-ray Photoelectron Spectroscopy (XPS)

Introduction

X-ray photoelectron spectroscopy, also known as ESCA (Electron Spectroscopy for Chemical Analysis), is the most widely used non-destructive surface analysis technique based upon the fundamental interactions of photons with matter viz., the photoelectric effect.[26,27] It provides the possibility to obtain information about the elemental composition, empirical formula, chemical state, and electronic state of the elements which are present within the material. The photoelectric effect was first discovered by Hertz in 1887[28] and later explained by Einstein in 1905.[29] After many years, Kai Siegbahn and his research group in Uppsala (Sweden) in 1954 recorded the first high-energy-resolution XPS spectrum of cleaved sodium chloride (NaCl), revealing the potential of XPS.[30] In 1969 some engineers together with Siegbahn produced the first commercial XPS instrument.

Theory

XPS is based on the photoelectric effect (**Figure 1.7**) in which a sample surface is irradiated with X-rays and photoelectrons are emitted. When an atom absorbs a photon of energy hν, a core or valence electron with binding energy E_b is ejected with kinetic energy E_k. $E_k = h\nu - E_b - \phi$, where h is Planck's constant, ν is the

frequency of the exciting radiation, E_b is the binding energy of the photoelectron relative to the Fermi level of the sample and ϕ is the work function of the

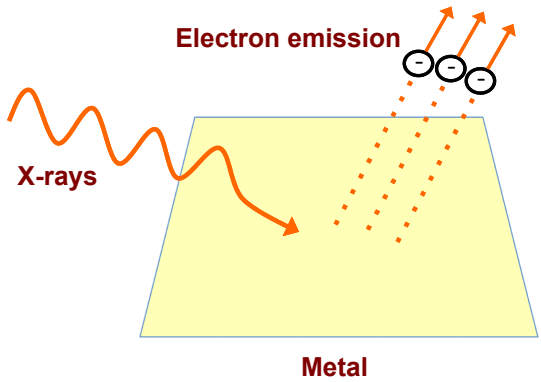

Figure 1.7 Illustration of photoelectric effect.

spectrometer. In XPS both core and valance electrons of the solid are emitted by using in-house laboratory X-ray sources (Al K_α (1486.6 eV) or Mg K_α (1253.6 eV)) or synchrotron radiation (produced by high-energy accelerated electrons). These X-ray sources have photon energies which are high enough to reach at least one core level of any element. Typically, the XPS spectrum is a plot of the intensity of photoelectrons versus binding energy. XP spectra allow an excellent elemental analysis of the target sample. This technique is surface sensitive since, the electrons whose energies are analysed in XPS arise from a depth of not greater than about 5 nm because the emitted photoelectrons have kinetic energy in the range of 50-100 eV and at this energy the value for inelastic mean free path for an electron is minimum. Each element has a characteristic set of binding energies and hence XPS can be used to analyse the composition of the samples.

Instrumentation

In the present study both laboratory instruments i.e where Al K_α radiation was used and a synchrotron-based light source of MAX-II ring of the MAX IV Laboratory were used. In the laboratory setup, X-ray photoelectron spectroscopy (XPS) was performed using a Physical Electronics Quantum 2000, which employs monochromatic Al K_α radiation, and was conducted under constant neutralization using an electron flood gun and very low energy Ar^+ ions (10 eV). This makes charge reference necessary. Thus, in the present work adventitious carbon was chosen and the binding energy of C 1s peak was referenced to 284.8 eV. Spectra

were obtained from the untreated surface of powder pressed into indium foil. The measurement spot had a diameter of 200 μm.

References

1. B.C. Gates, F.C. Jentoft, T. Takei, T. Akita, I. Nakamura, T. Fujitani, M. Okumura, K. Okazaki, J. Huang, T. Ishida, M. Haruta, *Advances in Catalysis, Ch. 1 Heterogeneous Catalysis by Gold*, Elsevier, 55, pp 1, **2012**; G.C. Bond, C. Louis, D.T. Thompson, *Catalysis by Gold, Ch.4 Preparation of Supported Gold Catalysts*, Imperial College Press, London, 6, pp 72, **2006**.
2. R. Jenkins, *''X-Ray Fluorescence Spectrometry'',* John Wiley & Sons, Inc. ISBN 0-471-83675-3, **1988**.
3. R. Jenkins, W. Gould, D. Gedcke, *Appl. Spectrosc. Rev.*, **2000**, 35(1,2), 129.
4. R. Jenkins, R. Gould, D. Gedcke, *''Quantitative X-ray Spectrometry''*, 2nd edition, Marcel Dekker, New York, **1995**.
5. R. Van Grieken, A. Markowicz, *''Handbook of X-Ray Spectrometry''*, Marcel Dekker, New York, **1993**.
6. R. Lachance, F. Claisse, *''Quantitative X-ray Fluorescence Analysis: Theory and Application''*, John Wiley, New York, **1995**.
7. J. Anzelmo, J. Lindsay, *Journal of Chemical Education*, **1987**, 64, A181.
8. J. Haber, *Pure Appl. Chem.*, **1991**, 63, 1227.
9. K. Sing, D. Everett, R. Haul, L. Moscou, R. Pierotti, F. Rouquerol, T. Siemieniewska, *Pure Appl. Chem*, **1985**, 57, 603.
10. S. Brunauer, P. Emmett, E. Teller, *J. Am. Chem. Soc.*, **1938**, 60, 309.
11. E. Barrett, L. Joyner, P. Halenda, *J. Am. Chem. Soc.*, **1951**, 73, 373.
12. R. Young (Ed.), *''The Rietveld Method''*, Oxford University Press, Oxford, **1993**.
13. W. H. Bragg, W. L. Bragg, *''The Crystalline State''*, Vol. 1, McMillan, New York, **1949**.
14. J. Fryer, *''Chemical Applications of Transmission Electron Microscopy''*, Academic Press, San Diego, **1979**.
15. D. Williams, C. Carter, *''Transmission electron microscopy, part 1: Basics''*, Springer 2nd ed., New York, **2009**.
16. A. Howie, in *''Characterization of Catalysts''*, Wiley, New York, p. 89, **1980**.

17. T. Baird, *''Characterization of Catalysts by Electron Microscopy, in Catalysis''*, Specialist Periodical Reports, The Royal Society of Chemistry, London, **1981**, 5, 172.

18. S. Chapman, *''Understanding and Optimizing electron Micrsocope Performance 1. Transmission Microscopy''*, Sci. Rev. Ltd. London, **1980**.

19. F. Delannay in *''Characterization of Heterogeneous Catalysts''* (Ed: F. Delannay), Dekker, New York, **1984**, 15, 71.

20. J. Sanders, *''The Electron Microscopy of Catalysts''*, in Catalysis: Science and Technology, Springer, Berlin, **1985**, 7, Ch. 2, 51.

21. A. Datye, *''The Study of Heterogeneous Catalysts by High-Resolution Transmission Electron Microscopy''*, Catal. Rec. Sci. Eng., **1992**, 34, 129.

22. P. Gallezot, C. Leclercq, in Catalyst Characterization; *''Physical Techniques for Solid Materials''* (Eds: B. Imelik. J. C. Vedrine), Plenum, New York, **1994**, Ch. 19, 509.

23. J. Stöhr: *'' X-ray Absorption: Principles, Application, techniques of EXAFS, SEXAFS, and XANES''*, R. Prins, New York, Wiley, **1988**; S. D. Kelly, D. Hesterberg, B. Ravel, *Analysis of soils and minerals using X-ray absorption spectroscopy, Methods of Soil Analysis– Part 5. Mineralogical Methods*, Soil Sci. Soc. Am., Madison, **2008**; G. Hähner, *Chem. Soc. Rev.*, **2006**, 35, 1244.

24. R. Nyholm, S. Svensson, J. Nordgren, and A. Flodström, *Nucl. Instr. Meth. Phys. Res. A*, **1986**, 246, 267.

25. J. Andersson, O. Björneholm, A. Sandell, R. Nyholm, J. Forsell, L. Thånell, A. Nilsson, and N. Mårtensson, *Synchr. Rad. New*, **1991**, 4, 15.

26. T. Carlson, *''X-Ray Photoelectron Spectroscopy''*, (Eds: D. Hutchinson, R. Stroudsburg), PA, **1978**.

27. D. Briggs, M. Seah (Eds.), *''Practical Surface Analyses, Vol. 1: Auger and X-Ray Photoelectron Spectroscopy''* (2nd Ed.), New York, **1990**.

28. H. Hertz, Ueber einen Einfluss des ultravioletten Lichtes auf die electrische Entladung. *Ann. Phys. (Berlin)*, **1887**, 267, 983.

29. A. Einstein, Generation and conversion of light with regard to a heuristic point of view, *Ann. Phys. (Berlin)*, **1905**, 17, 132.

30. K. Siegbahn, K. Edvarson, β-Ray spectroscopy in the precision range of $1{:}1e6^{II}$, *Nuclear Physics*, **1956**, 1 (8), 137.

Chapter 2. Sonogashira Coupling over Supported Gold Nanoparticles and Au (111) Surface

2.1 Introduction

Sonogashira cross-coupling is a unique method for the coupling between *sp* and sp^2 or sp^3 carbon atoms under mild reaction conditions.[1-4] In 1975 Sonogashira[5] discovered it and it attracted great interests from polymer and pharmaceutical industries.[6,7] For example, the Terbinafine drug, which is used as an antifungal agent is synthesised by the Sonogashira coupling reaction.[8]

In homogeneous reaction conditions palladium complexes are used to catalyze the Sonogashira reaction. The original Sonogashira catalyst was composed of $Pd(PPh_3)_2Cl_2$ with CuI as a co-catalyst, and leading to high conversion and selectivity to the cross-coupled product.[5] The use of copper salts as co-catalysts has an advantage in that it allows an increase in reaction rate, but on the other hand, its presence in the reaction also has a few disadvantages. First, it gives alkyne dimers, which upon oxidation generate the homocoupling product of the alkyne making it necessary to run the reaction in an inert atmosphere. Second, in standard conditions a high loading of palladium is required. Therefore, to overcome these problems, research has been focused on using homogeneous, Cu-free palladium catalysts with reduced Pd-loading. In this regard, several Pd complexes have been reported.[9-12] Nevertheless, the general issues associated with homogeneous catalysis such as recycling and separation are present and, thus, it would be advantageous to develop a heterogeneous catalyst. In this direction, different molecular complexes of palladium as well as other metals have been heterogenized on suitable carriers (Pd-NHC/γ-Fe_2O_3, $Pd(OAc)_2$/MCM-41, Pd/MOF, Au(I) and Au(III)/MCM-41, Rh/γ-alumina and nano CuO) and evaluated in the Sonogashira coupling reaction.[13-19] However, these catalysts usually suffer

from excessive leaching of the active metal, low conversion and poor selectivity for the desired hetero-coupled product.

Recently, supported gold nanoparticles have been shown as highly selective and superior catalysts for various important organic transformations[20-26] including the Sonogashira coupling reaction.[27-29] There are different suggestions regarding the active species involved in the Sonogashira coupling reaction.[27,30] It is well known that the size of gold nanoparticles has an influential role on their performance in various organic reactions.[20] In supported gold nanoparticles, the type of synthetic route chosen for the preparation of the catalyst and the nature of the support employed as the carrier can affect the particle size of the gold and the nature of the Au species. Therefore, we have investigated the impact of preparation methods and carriers on the characteristics and performance of supported gold nanoparticles for the Sonogashira cross coupling. In addition, to shed light on the mechanism involved in Sonogashira reaction we have performed XPS and XAS studies over Au(111).

2.2 Synthesis of CeO_2, TiO_2, and Al_2O_3 supported Au nanoparticles

The gold precursor, $HAuCl_4 \cdot xH_2O$, and carriers (CeO_2, TiO_2, and Al_2O_3) with different properties such as redox and non-redox character were employed. Supported gold nanoparticles were prepared by two different synthesis methods: (i) deposition-precipitation (DP) and (ii) incipient wetness impregnation (IMP) (**Chapter 1**). The nominal gold content in all preparations was constant (3 wt.%). Hereafter, the catalyst obtained after calcination, are denoted by adding DP (for deposition-precipitation) or IMP (for incipient wetness impregnation) to their names, for e.g., Au/CeO_2 prepared by DP and IMP routes will be designated as Au/CeO_2-DP and Au/CeO_2-IMP, respectively.

2.3 Characterisation of CeO_2, TiO_2, and Al_2O_3 supported Au nanoparticles

The synthesised catalysts were thoroughly characterised using X-ray fluorescence (XRF), N_2-sorption, X-ray diffraction (XRD), X-ray photoelectron spectroscopy (XPS), high-resolution transmission electron microscopy (HRTEM), and energy dispersive X-ray spectroscopy (EDX) techniques, which are described in **Chapter 1**.

XRF analysis revealed that the gold loading was in the range of 2.7-2.9 wt.% (**Table 1**), in all the samples that is close to the nominal gold loadings of 3 wt.%. The specific surface area (S_{BET}) of all the catalysts was similar to their corresponding pristine carriers, which indicates that the gold is deposited on the surface of the metal oxide.

Tabel 1 Characterisation data of catalysts.

Catalyst	Au content[a] (Wt.%)	Au content[b] (Wt.%)	S_{BET} (m^2g^{-1})	Average Au size[d] (nm)
Au/CeO_2-DP	2.8	0.62	53(57)	4.4
Au/TiO_2-DP	2.7	0.58	50(54)	13.7
Au/Al_2O_3-DP	2.8	0.39	189(190)	4.4[4][e]
Au/CeO_2-IMP	2.8	0.54	45(57)	50[115]
Au/TiO_2-IMP	2.8	0.55	49(54)	55[113]
Au/Al_2O_3-IMP	2.9	0.38	181(190)	96[98]

[a] Au content in as-prepared catalysts determined by XRF.

[b] Au content after 160 h catalytic run determined by XRF.

[c] Surface area of pristine supports in round brackets.

[d] Determined from HRTEM/TEM images.

[e] Au crystallite size estimated applying Scherrer equation to X-ray diffractograms in square bracket.

Powder X-ray diffractogram of samples prepared by the DP method shows very weak reflections belonging to the gold species for Au/CeO_2-DP and Au/TiO_2-DP compared to Au/Al_2O_3-DP. Furthermore, the position of Au reflections matched well with the reference lines specific for metallic gold (ICSD 44362), indicating that metallic gold is formed on all of the three carriers.[31,32] The powder X-ray diffractograms for the catalysts prepared by incipient wetness impregnation shows sharp reflections corresponding to metallic gold for all of the three systems, Au/CeO_2-IMP, Au/TiO_2-IMP, and Au/Al_2O_3-IMP.[31,32] The sharp reflections due to gold indicates that the impregnation preparation route led to much larger gold particles as compared to the deposition-precipitation (**see details in Chapter 1**).

XPS study indicates the presence of metallic Au(0) species also at the surface level. However, the peaks are slightly shifted to lower value by ca. 0.5 eV compared to those reported for metallic Au in the literature.[30,33] This shift could be a result of metal particle quantum size effect, which can lead to a shift in the range of 0.6-1 eV.[30,34] Moreover, the two components in the Au 4*f* XP spectra are separated by 3.7 eV which is in very good agreement with the reported value for

metallic Au and not 2.5 eV which is reported for Au(I) and Au(III) molecular compounds.[33,35]

From HRTEM the morphology and textural properties of supported gold nanoparticles were investigated. Au/CeO_2-DP show small gold nanoparticles with mean particle size of 4.4 nm (±1.5 nm), Au/TiO_2-DP shows Au nanoparticles with mean particle size of 13.7 nm (±2.8 nm), and in the case of Au/Al_2O_3-DP gold nanoparticles have an average particle size of 4.4 nm (± 2 nm). The impregnated samples display gold particles in the broad range of 20-200 nm, with average particle size of 50, 55, and 96 nm, respectively. This indicates substantial agglomeration of gold in the IMP route, in line with the XRD results.

2.4 Catalytic activity in Sonogashira coupling reaction over supported Au catalyst

Sonogashira coupling of PA and IB was carried out with supported gold catalyst synthesised by both DP and IMP method. In a typical reaction run PA (0.5 mmol), IB (0.5 mmol), and K_2CO_3 (0.3 mmol) was added to the solvent (DMF) and kept

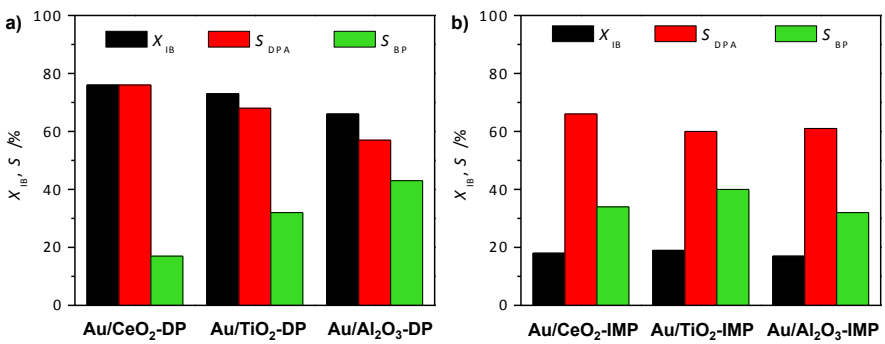

Figure 2.1. Iodobenzene conversion (X_{IB}) and selectivity (S) in Sonogashira coupling reaction between PA and IB over supported gold nanoparticles. a) Catalysts synthesised by DP and b) catalysts synthesised by IMP. Reaction conditions are detailed in the section 2.4.

for stirring at 145°C for 160 h. The obtained results are shown in **Figure 2.1a,b**.

Catalysts synthesised by the DP method i.e Au/CeO_2-DP, Au/TiO_2-DP, and Au/Al_2O_3-DP show high conversion (76%, 73%, and 66%) and selectivity for DPA (76%, 68%, and 57%) as compared to catalysts synthesised by the IMP method. In addition, IMP synthesised catalysts show IB conversion of ca. 18%. These results clearly suggest that the deposition-precipitation method is highly superior to the incipient wetness impregnation as the catalysts prepared with the

former route provide the highest conversion and selectivity. Among all the synthesised catalysts Au/CeO_2-DP gives the highest IB conversion and selectivity for DPA.

If we compare the influence of the carriers on catalyst performance it is noticed that the Au nanoparticles supported on carriers with redox properties (CeO_2 and TiO_2) lead to higher conversion and selectivity compared to the non-redox Al_2O_3 carrier. This is particularly distinct for the catalysts synthesised by the DP route. Au/CeO_2-DP and Au/Al_2O_3-DP feature Au nanoparticles of 4.4 nm, but the former displays a significantly better IB conversion and DPA selectivity than the latter (**Figure 2.1a**). However, Au/CeO_2-DP and Au/TiO_2-DP possess Au nanoparticles of different size (4.4 versus 13.7 nm) but lead to similar activities and a slightly lower DPA selectivity for the latter. Overall, these results indicate that for redox supports the Au particle size effect on the catalyst performance is not noticeable in the range of 4-14 nm. In case of the catalyst synthesised by the IMP route they have bigger particles (~100 nm) and they all lead to similar IB conversion and DPA selectivity (**Figure 2.1b**).

To know the effect of particle size on activity of catalysts, we plotted a graph of IB conversion and DPA selectivity versus the particle size of gold for Au/CeO_2 samples, selected as an example (**Figure 2.2**). It can be seen that the catalyst with

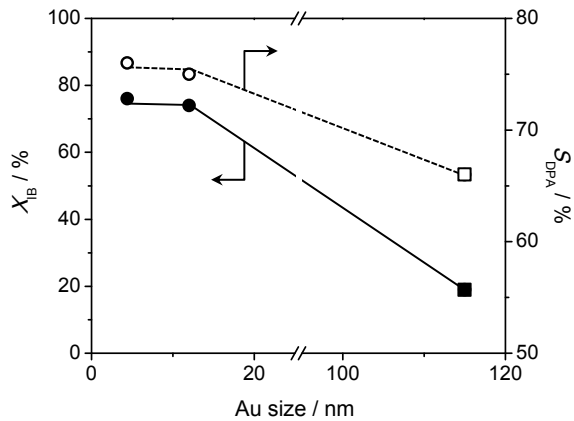

Figure 2.2. Influence of Au particle size on IB conversion (X_{IB}, solid lines) and DPA selectivity (S_{DPA}, dashed lines) for Au/CeO_2 samples. Circles represent catalysts prepared by DP route, while squares denotes samples obtained by IMP method. Lines are only intended as guides to the eye. Reaction conditions are detailed in the Section 2.4.

smaller Au particle size in the range of 4-14 nm exhibited similar and high IB conversion. Thus, is most likely due to the high degree of dispersion expected for

smaller particles, providing higher number of active sites for the reaction to take place. Likewise, the DPA selectivity is similar and higher until 14 nm but afterwards it drops. If we compare the Au particle size data in **Table 1** and reaction results in **Figure 2.1a,b** for Au/TiO_2 and Au/Al_2O_3 similar results can be obtained. Hence, it can be concluded that the gold nanoparticles supported on redox supports with the Au particle size in the range of 3-15 nm show similar reactivity, while bigger nanoparticles (>15 nm) lead to inferior performance.

A gold leaching study was performed with all the catalyst and the extent of gold leaching was determined by XRF of the used catalyst after 160 h catalytic run and shown in **Table 1**. Similar Au leaching (78-80%) was observed with Au/CeO_2 and Au/TiO_2 samples, prepared by DP and IMP, while Au/Al_2O_3 (DP and IMP) showed slightly higher gold leaching of 86%. These results suggest a severe gold loss during catalysis, in accordance with previous results in DMF solvent.[27,28] Thus, it seems that in the leaching process catalyst synthesis route and particle size play no significant role. Regardless, of the extensive leaching the conversion follows first order behaviour during the whole reaction and the reaction is clearly heterogeneous as the conversion ceases in the solution after hot filtration.

2.5 Insights into Sonogashira coupling via in-situ surface studies over Au(111)

All the experiments i.e XPS and XAS measurements were performed at beamline D1011 of the MAX-II ring of the Swedish synchrotron radiation facility at the MAX IV Laboratory.

To understand the mechanism of Sonogashira coupling reaction, dosing of halogenated benzene (iodobenzene, chlorobenzene, and bromobenzene) and phenylacetylene (PA) on a Au(111) crystal was performed. The halogenated benzenes and phenylacetylene were cleaned by freeze-pump-thaw cycles prior to dosing upon the cleaned Au(111) crystal.

Adsorption of the three different halogenated benzene (Cl-, Br-, and I-benzene) and phenylacetylene shows that iodobenzene and chlorobenzene dissociate and hence, Sonogashira coupling is possible. On the other hand, bromobenzene does not dissociate and also gave no coupling product.

2.6 Conclusions

Gold nanoparticles on supports of different nature (redox: CeO_2, TiO_2 and non-redox: Al_2O_3) have been synthesised using deposition-precipitation and incipient wetness impregnation. XRD and XPS study revealed that the catalyst synthesized by both methods incorporate gold on all the carrier and in all the samples gold is present in metallic state. Small Au nanoparticles were obtained with the DP route, while the IMP method leads to larger agglomerates, an agglomeration that is most likely caused by the presence of chlorine species during calcination. The catalysts synthesized by DP route shows better conversion and cross-coupling selectivity in the Sonogashira coupling between phenylacetylene and iodobenzene due to the formation of highly dispersed and smaller Au nanoparticles. Especially CeO_2 and TiO_2 supported samples showed better performance than Al_2O_3 supported ones. On the other hand, catalysts synthesised by IMP route shows no difference in the reactivity. The catalyst performance is not dependent on the average gold particle size in the range of 3-15 nm, but above this range the catalyst performance changes, as demonstrated for the case of Au/CeO_2 system. Moreover, the leaching of gold is independent of gold particle size and preparation method. Adsorption of halo benzenes (chloro-, bromo-, and iodobenzene) with phenylacetylene on Au(111) surface shows that iodobenzene and chlorobenzene desorb after dissociation and gave homocoupling product (biphenyl), however, bromobenzene doesn't show any dissociation and that is why no coupling product is observed.

References

1. N. Miyaura, K. Yamada, A. Suzuki, *Tetrahedron Lett.*, **1979**, 20, 3437.
2. R. F. Heck, J. P. Nolley, *J. Org. Chem.,* **1972**, 37, 2320.
3. E. Negishi, A. O. King, N. Okukado, *J. Org. Chem.*, **1977**, 42, 1821.
4. H. Tokuyama, S. Yokoshima, T. Yamashita, S. C. Lin, L. Li, T. Fukuyama, *J. Braz. Chem. Soc.*, **1998**, 9, 381.
5. K. Sonogashira, Y. Tohda, N. Hagihara, *Tetrahedron Lett.*, **1975**, 16, 4467.
6. G. Altenhoff, S. Würtz, F. Glorius, *Tetrahedron Lett.*, **2006**, 47, 2925.
7. K. C. Nicolaou, W. M. Dai, *Angew. Chem. Int. Ed.*, **1991**, 30, 1387.
8. A. O. King, N. Yasuda, *Top. Organomet. Chem.*, **2004**, 6, 205.
9. S. Cacchi, E. Morera, G. Ortar, *Synthesis*, **1986**, 4, 320.
10. M. R. Buchmeiser, T. Schareina, R. Kempe, K. Wurst, *J. Organomet. Chem.*, 2001, 634, 39.
11. C. Nájera, J. Gil-Moltó, S. Karström, L. R. Falvello, *Org. Lett.*, **2003**, 5, 1451.
12. W. A. Herrmann, *Angew. Chem. Int. Ed.*, **2002**, 41, 1290.
13. P. D. Stevens, G. Li, J. Fan, M. Yenb, Y. Gao, *Chem. Commun.*, **2005**, 35, 4435.
14. K. Komura, H. Nakamura, Y. Sugi, *J. Mol. Catal. A: Chem.*, **2008**, 293, 72.
15. S. Gao, N. Zhao, M. Shu, S. Che, *Appl. Catal. A: Gen.*, **2010**, 388, 196.
16. A. Corma, C. González-Arellano, M. Iglesias, S. Pérez-Ferreras, F. Sánchez, *Synlett*, **2007**, 11, 1771.
17. C. González-Arellano, A. Corma, M. Iglesias, F. Sánchez, *Eur. J. Inorg. Chem.*, **2008**, 7, 1107.
18. V. K. Kanuru, S. M. Humphrey, J. M. W. Kyffin, D. A. Jefferson, J. W. Burton, M. Armbrüster, R. M. Lambert, *Dalton Trans.*, **2009**, 7602.
19. Y. Yuan, H. Zhu, D. Zhao, L. Zhang, *Synthesis*, **2011**, 1, 1792.
20. A. S. K. Hashmi, G. J. Hutchings, *Angew. Chem. Int. Ed.*, **2006**, 45, 7896.
21. M. Haruta, *Catal. Today*, **1997**, 36, 153.
22. E. Tebandeke, C. Coman, K. Guillois, G. Canning, E. Ataman, J. Knudsen, L. R. Wallenberg, H. Ssekaalo, J. Schnadt, O. F. Wendt, *Green Chem.*, **2014**, 16, 1586;

D. K. Dumbre, P. N. Yadav, S. K. Bhargava, V. R. Choudhary, *J. Catal.*, **2013**, 301, 134.

23. P. Serna, A. Corma, *ChemSusChem*, **2014**, 7, 2136.
24. Y. Zhang, X. Cui, F. Shi, Y. Deng, *Chem. Rev.*, **2012**, 112, 2467.
25. M. Stratakis, H. Garcia, *Chem. Rev.*, **2012**, 112, 4469.
26. B. Takale, M. Bao, Y. Yamamoto, *Org. Biomol. Chem.*, 2014, 12, 2005.
27. C. Gonzlez-Arellano, A. Abad, A. Corma, H. García, M. Iglesias, F. Sánchez, *Angew. Chem. Int. Ed.*, **2007**, 46, 1536.
28. G. Kyriakou, S.K. Beaumont, S.M. Humphrey, C. Antonetti, R.M. Lambert, *ChemCatChem*, **2010**, 2, 1444.
29. A. Corma, R. Juárez, M. Boronat, F. Sánchez, M. Iglesias, H. García, *Chem. Commun.*, **2011**, 47, 1446.
30. S. K. Beaumont, G. Kyriakou, R. M. Lambert, *J. Am. Chem. Soc.*, **2010**, 132, 12246.
31. V. S. Narkhede, A. Toni, V. V. Narkhede, M. Guraya, J. W. Niemantsverdriet, M. W. E. Van den Berg, W. Grünert, H. Gies, *Micropor. Mesopor. Mat.*, **2009**, 118, 52.
32. C. Wang, C. Chien, Y. Yu, C. Liu, C. Lee, C. Chen, Y. Hwu, C. Yang, J. Je, G. Margaritondo, *J. Synchrotron Rad.*, **2007**, 14, 477.
33. T. D. Thomas, P. Weightman, *Phys. Rev. B*, **1986**, 33, 5406.
34. A. K. Santra, D. W. Goodman, *J. Phys. Condens. Matter*, **2003**, 15, 2, R31.
35. J. F. Moulder, W. F. Stickle, P. E. Sobol, K. D. Bomben, In Handbook of *X-ray Photoelectron Spectroscopy*, Physical Electronics, Inc., Eden Prairie, Minnesota, USA, **1995**.

Chapter 3. Styrene Epoxidation over Gold Nanoparticles Supported on Mesoporous Materials

3.1 Introduction

Epoxides are very useful intermediates for synthesis of fine chemicals. They are obtained by olefin epoxidation using H_2O_2, dioxygen, and commercially available peroxyacids.[1-3] Peroxyacids are very hazardous to handle and generate a lot of liquid waste.[4,5] On the contrary, H_2O_2 and dioxygen are green oxidant but they usually suffer from low alkene conversion and poor control of selectivity which results in a low yield of desired epoxide.[1-3] These problems associated with peroxyacids, H_2O_2, and dioxygen can be reduced by replacing them with organic hydroperoxides.[6]

Olefin epoxidation especially styrene epoxidation is of great interest because it generates styrene oxide which has numerous application, in the production of styrene glycol and its derivatives, as a raw material for the production of phenethyl alcohol used in perfumes, and as a chemical intermediate for cosmetics.[7] Various catalysts (Ti/SiO_2, $Si\text{-}Ti/SiO_2$, Ts-1, Au/alumina and Au/TiO_2) have been used in styrene epoxidation.[8-11] However, they are unable to give high activity with low metal loadings. Therefore, it is of great interest to investigate new class of catalysts.

In this context, Choudhary *et al.* and Dumbre *et al.* have reported that nano-gold supported on metal oxides synthesised by the homogeneous deposition-precipitation method are promising catalysts for the epoxidation of styrene by using TBHP as an oxidant.[12,13] Jin *et al.* have synthesised a periodic mesoporous organosilica incorporated with bridging disulfide-imidazolium units loaded with gold.[14] So far, the best catalyst has been obtained by Liu et al. which is, Au_{25} clusters supported on hydroxyapatite.[15] It gives full styrene conversion by using

TBHP as an oxidant with 92% selectivity for styrene oxide in 12 h and selectivity drops after 12 h.

Periodic mesoporous silica materials, such as SBA-15 and MCM-41, have been used as supports for gold, in styrene oxidation using dioxygen or H_2O_2 as oxidant. These supports have significantly improved the performance of the gold-based catalysts.[16-18] Noteworthy is that this types of periodic mesoporous silica carriers have not been thoroughly studied for epoxidation of styrene using TBHP as oxidant, which, potentially offers a better control on the epoxide selectivity.

3.2 Synthesis of mesoporous material supported gold nanoparticles

Gold nanoparticles supported on porous materials (MCM-41, SBA-15, KIT-6, and SiO_2) were synthesised by the deposition-precipitation method (DP) (**Chapter 1**). Hereafter, the catalysts are denoted by adding the support name to Au for e.g., Au/MCM-41, Au/SBA-15, Au/KIT-6, and Au/SiO_2.

3.3 Characterisation of catalysts

All the synthesised catalysts were characterised by XRF, PXRD, N_2 sorption, and High angle annular dark-field scanning transmission electron microscopy (HAADF-STEM) (**Chapter 1**)

To confirm the mesoporous characteristics of supports, the supports were calcined and characterised by N_2 sorption. MCM-41, SBA-15, and KIT-6 show type IV isotherms characteristic of mesoporous material.[19] On the other hand, fumed silica

Table 1. Characterisation data of the catalysts.

Catalyst	Au content[a] (Wt.%)	Porous properties[b]	
		S_{BET}[c] (m^2g^{-1})	V_{pore}[d] (cm^3g^{-1})
Au/MCM-41	1.0	774 (840)[e]	0.82 (0.91)[f]
Au/SBA-15	0.9	449 (512)	0.86 (0.95)
Au/KIT-6	1.1	540 (753)	0.88 (0.95)
Au/SiO_2	1.0	193 (195)	0.61 (0.62)

[a]Determined by XRF.

[b]Determined by N_2 sorption.

[c]Total surface area determined using BET method.

[d]Total pore volume, [e & f] Porous properties of corresponding supports in brackets.

used for comparative purposes, shows the isotherm which might fit to type II that is typical for nonporous materials. In addition, the surface area for fumed silica is much lower than for the other three carriers (**Table 1**). Supported gold catalysts were also characterised by N_2 sorption. In case of Au/MCM-41, Au/SBA-15, and Au/KIT-6 there is a decrease in surface area after gold deposition which indicates that gold might have deposited inside the pores. This is in accordance with the drop in the total pore volume (V_{pore}) of these catalysts compared to their corresponding carriers (**Table 1**). However, there is no considerable change in S_{BET} and V_{pore} of SiO_2 upon gold loading, suggesting that the gold deposition is on its surface. The gold loading determined by XRF for all the catalyst is in the range of 0.9-1.1 wt.%. The powder X-ray diffractograms of Au/MCM-41, Au/SBA-15, Au/KIT-6, and Au/SiO_2 showed reflections due to gold which are matched well with the reference line for Au(0) (ICSD 44362).

HAADF-STEM of Au/MCM-41 showed gold particles size in the range of 2-5 nm. However, HAADF-STEM of Au/SBA-15, Au/KIT-6, and Au/SiO_2 displayed larger Au particles in the range of 10-30 nm. Therefore, it seems that MCM-41 with the largest surface area, enables the highest dispersion and stabilises the small Au nanoparticles on its surface better than other carriers of this study.

3.4 Catalytic activity in epoxidation of styrene

The catalytic activity of periodic mesoporous material supported gold nanoparticles was evaluated in styrene epoxidation at 80°C using TBHP as an oxidant and acetonitrile as a solvent. Two products were obtained namely: the desired styrene oxide (SO) and the side product benzaldehyde (BZ). The catalytic activity performances of all the catalysts are shown in **Figure 3.1a**. Au/MCM-41 led to the highest styrene conversion ($X_{Styrene}$) of 41% and selectivity to styrene oxide (S_{SO}) of 96%, followed by Au/SBA-15 ($X_{Styrene}$ = 30%, S_{SO} = 90%), Au/KIT-6 ($X_{Styrene}$ = 25%, S_{SO}= 86%), and SiO_2 ($X_{Styrene}$ = 30%, S_{SO} = 95%).

To elucidate the difference in catalytic activity, different properties were considered such as gold content, surface area, and the nature of gold species. However, none could explain the difference in activity. However, the particle size determined by HAADF-STEM places the materials in two classes: one with particle size in the range of 2-5 nm (Au/MCM-41), and other with particle size in the range of 10-30 nm (other three catalyst). Therefore, we have plotted gold mean particle size versus styrene conversion and styrene oxide selectivity (**Figure 3.1b**).

The smallest Au particle size catalyst (Au/MCM-41) shows the highest activity and the highest Au particle size catalyst (Au/KIT-6) shows the lowest activity. Thus, the control of gold particle size is a key to achieve the best performance in

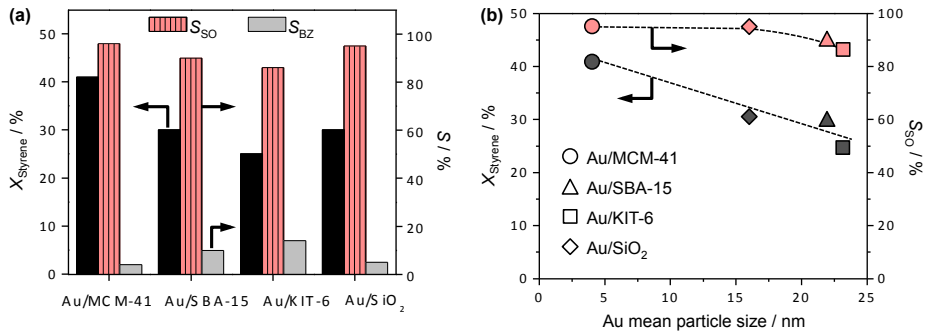

Figure 3.1 (a) Styrene conversion ($X_{Styrene}$) and selectivity (S) in styrene epoxidation over different mesoporous material supported gold catalysts. (b) Correlation of $X_{Styrene}$ and styrene oxide selectivity (S_{SO}) with mean particle size of gold nanoparticles in different catalysts, determined from HAADF-STEM analysis. S_{SO} = selectivity to styrene oxide and S_{BZ} = selectivity to benzaldehyde.

the selective styrene oxidation. The best catalyst i.e Au/MCM-41 was used in optimisation of reaction parameters such as: influence of temperature, influence of time, influence of solvent, influence of oxidant, and the effect of TBHP:Styrene ratio.

3.5 Conclusions

Mesoporous material (MCM-41, SBA-15, KIT-6, and SiO_2) supported gold nanoparticles were synthesised by the deposition-precipitation method. The catalysts were characterised by XRF, PXRD, N_2 sorption, and HAADF-STEM. Furthermore, the catalytic activity was evaluated in the styrene epoxidation at 80°C using TBHP as oxidant and acetonitrile as solvent. N_2 sorption and XRF confirms the incorporation of gold (ca. 1 wt.%) onto all mesoporous carriers and the presence of gold in metallic form in all the catalysts. Because of its lowest gold nanoparticles size, Au/MCM-41 gives the highest styrene conversion (41%) and styrene oxide selectivity (96%) just after 1 h of reaction. The optimisation of reaction parameters such as temperature reveals that conversion and selectivity increases with increase in temperature from 60-80°C and further increase in temperature is detrimental, the time study shows there is an induction period as the rate of the reaction in the first 0.5 h is very slow, but increases abruptly in the next

0.5 h. The induction time is attributed to the time needed for the generation of peroxide radical from TBHP, however, no positive improvement is observed by using different oxidants and solvents, but TBHP:styrene ratio shows that 1-1.6 is good to achieve a high styrene conversion and high styrene oxide selectivity.

References

1. L. Wang, B. Zhang, W. Zhang, J. Zhang, X. Gao, X. Meng, D. S. Su, F. S. Xiao, *Chem. Commun.*, **2013**, 49, 3449.
2. Y. Zheng, X. Zhang, Y. Yao, X. Chen, Q. Yang, *RSC Adv.*, **2015**, 5, 105747
3. A. S. Sharma, D. Shah, H. Kaur, *RSC Adv.*, **2015**, 5, 42935.
4. J. Judge, *Organic peroxides*, Wiley Interscience, New York, **1971**.
5. M. Sittig, *Handbook of Toxic and Hazardous Chemicals and Carcinogens*, 2nd ed., Noyes Publications, Park Ridge, New Jersey, **1985**.
6. R. Hiatt, G. Howe, *J. Org. Chem.*, **1971**, 36, 2493.
7. F. Ullmann, *Ullmann's Encyclopedia of Industrial Chemistry*, 6th edn, (Electronic Release), Wiley/VCH, New York, **1998**.
8. Q. Yang, S. Wang, J. Lu, G. Xiong, Z. Feng, X. Xin, C. Li, *Appl. Catal. A: Gen.*, **2000**, 194, 507.
9. R. V. Grieken, J. L. Sotelo, C. Martos, J. L. G. Fierro, M. Lopez-Granados, R. Mariscal, *Catal. Today*, **2000**, 61, 49.
10. D. Yin, L. Qin, J. Liu, C. Li, Y. Jin, *J. Mol. Catal. A: Chem.*, **2005**, 240, 40.
11. N. S. Patil, B. S. Uphade, P. Jana, R. S. Sonawane, S. K. Bhargava, V. R. Choudhary, *Catal. Lett.*, **2004**, 94, 89.
12. V. R. Choudhary, D. K. Dumbre, *Top. Catal.*, **2009**, 52, 1677.
13. D. K. Dumbre, V. R. Choudhary, N. S. Patil, B. S. Uphade, S. K. Bhargava, *J. Colloid Interface Sci.*, **2014**, 415, 111.
14. Y. Jin, P. Wang, D. Yin, J. Liu, H. Qiu, N. Yu, *Micropor. Mesopor. Mater.*, **2008**, 111, 569.
15. Y. Liu, H. Tsunoyama, T. Akita, T. Tsukuda, *Chem. Commun.*, **2010**, 46, 550.
16. N. Linares, C. P. Canlas, J. Garcia-Martinez, T. Pinnavaia, *Catal. Commun.*, **2014**, 44, 50.
17. J. Wei, L. Zou, *Chem. Lett.*, **2016**, 45, 567.
18. M. Turner, V. Golovko, O. Vaughan, P. Abdulkin, A. Berenguer-Murcia, M. Tikhov, B. Johnson, R. M. Lambert, *Nature*, **2008**, 454, 981.
19. J. Liu, J. Yang, Q. Yang, G. Wang, Y. Li, *Adv. Funct. Mater.*, **2005**, 15, 1297.

Chapter 4. Oxidative Cross-Coupling Reaction Catalysed by Au/ZrO_2

4.1 Introduction

Transition metal catalysed, oxidative C-C coupling reaction to form biaryls have attracted researchers, because biaryls are important structural motifs in natural products, pharmaceuticals, agrochemicals and materials.[1-4] The standard method for synthesis of biaryls is metal-mediated coupling reactions of the pre-activated aryl substrate.[5-7] However, this standard procedure has a few disadvantages for example: (i) pre-activation such as halogenation or sulfonate formation increases the number of synthesis steps in formation of the final product, (ii) difficulty in the availability of activating group, and (iii) preactivation step generates a lot of waste from solvents, reagents, and chromatographic purification of the products. Therefore, to prevail over these drawbacks one possibility could be a direct arylation process, which involves direct coupling of non-activated C-H bonds with activated or non-activated arenes.

There has been growing interest in oxidative coupling of non-activated arenes through direct arylation.[8] In reference to this, Pd, Rh, and Ru metal complexes are the most frequently used catalysts.[9-11] Oxidative coupling catalysed by Lewis acid has also been studied and addition of Lewis acid has been shown to increase the selectivity.[12] However, the direct arylation of non-activated arenes has not reached its optimum level because practically the catalytic systems should be less expensive, highly efficient, and environmentally friendly. Many recent studies have focused on the development of arylation of arenes such as: coupling of indoles (functionalised and unfunctionalised), benzofuran, pentafluorobenzene with benzene in presence of oxidant,[13-15] and microwave assisted coupling of indoles with benzene.[16] However, all these reactions require inert atmosphere, harsh reaction conditions, and special metal additives to enhance reactivity and selectivity. Therefore, there is a need of suitable catalyst that can clear up all the pointed issues.

The catalysis with gold has been extensively studied after the discovery of its activity in different chemical reactions.[17,18] Recently, gold salts (homogenous catalyst) and supported gold nanoparticles (heterogeneous catalyst) have shown activity in oxidative coupling of non-activated arenes for example: Kar et al. have shown that catalytic amount of soluble gold salts can catalyse the coupling of non-activated arenes to biaryl by using hypervalent iodine compounds as an oxidant.[19] Very recently, Serana and Corma have reported intramolecular coupling of non-activated arenes by supported gold nanoparticles.[20] However, there are no studies with heterogeneous catalyst on intermolecular oxidative cross coupling reaction of non-activated arenes to obtain heterocoupled product selectively. Therefore, it encouraged us to explore the catalytic activity of supported gold nanoparticles in this reaction.

4.2 Synthesis of catalysts

The catalysts were synthesised by deposition-precipitation method described in **Chapter 1**. The nominal gold loading was fixed to 3 wt.%. $HAuCl_4 \cdot xH_2O$ is the gold precursor used in preparation and supports ZrO_2, TiO_2, and Al_2O_3 were used as received. Henceforth, the catalysts will be denoted as Au/ZrO_2, Au/TiO_2, and Au/Al_2O_3. Au/TiO_2, and Au/Al_2O_3 have been used for comparison purpose.

4.3 Characterisation of Au/ZrO_2

To study the surface and bulk properties of the catalysts all the catalysts were characterised by different techniques like, XRF, Powder X-ray diffraction, N_2 sorption, XPS, and TEM.

The gold loading obtained by XRF is same for all the catalysts i.e 2.7 and 2.8 wt% which is close to nominal gold loading of 3 wt%. Supported gold catalysts showed decrease in surface area, which indicates the successful deposition of gold on support.

Powder X-ray diffraction patterns for Au/ZrO_2 and Au/TiO_2 show small and broad reflections due to gold. However, Au/Al_2O_3 shows broad reflections due to gold and they are clearly visible because of the low crystallinity of the Al_2O_3 carrier.

Presence of small and broad reflections due to gold hints to the presence of gold as small nanoparticles. All reflections are matched well with Au(0).

The XPS spectra for the Au 4f shows two peaks at 83.4 eV and 87.1 eV for Au $4f_{7/2}$ and Au $4f_{5/2}$ which is due to Au(0) species.

Representative TEM micrographs were acquired in order to measure the particle size distributions which is in the range of 4-14 nm. The average particle size for Au/ZrO_2, Au/TiO_2, and Au/Al_2O_3 is 4 nm, 13.7 nm, and 4.4 nm.

4.4 Oxidative cross-coupling of non-activated arenes

The generalised scheme for oxidative coupling is shown in **Scheme 4.1**. To examine the catalytic activity of catalysts the oxidative cross-coupling of 4-bromoanisole (10 mmol) with benzene (5mmol) was carried out at 100°C for 24 h by using $PhI(OAc)_2$ (1mmol), acetic acid (2 ml) as oxidant and solvent. Blank reaction shows no activity which shows the importance of the catalyst. By using

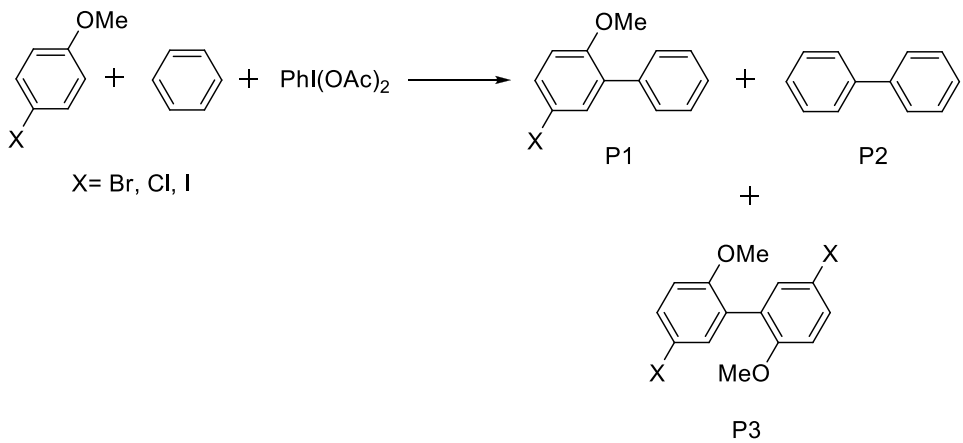

Scheme 4.1 Generalized scheme for Oxidative cross coupling of non-activated arenes.

our reaction conditions three products were formed, P1 the heterocoupling product, P2 (biphenyl), P3 homocoupling product of halo-anisole. Screening of the catalysts show that Au/ZrO_2 is the best catalyst giving 4-bromoanisole conversion (X_{BA}) = 18% and ratio for the products are P1:P2:P3= 58:40:2 as compared to Au/TiO_2 (X_{BA}= 11%, P1:P2:P3= 49:49:2) and Au/Al_2O_3 (X_{BA}=2%, P1:P2:P3= 45:54:1). However, we noted that with the reaction conditions used in this study theoretically the maximum bromoanisole conversion which we can get is 10% at full oxidant conversion. But we are getting 18% and 11% for Au/ZrO_2 and

Au/TiO_2 that is more than 100% and this issue could be solved either by using a different oxidant such as Mes-I$(OAc)_2$ or by calculating oxidant (PhI$(OAc)_2$) conversion. However, it is not possible to calculate oxidant conversion from GC and this oxidant is exceptional because other oxidants like TBHP, H_2O_2, $K_2S_2O_8$, and Oxone® gave no activity. Further, it has been observed in our previous work that phenyl iodide (obtained after dissociation of oxidant) can couple with itself in the presence of supported gold catalyst to give homocoupling product i.e biphenyl.

Different halo-anisoles (Cl-anisole and I-anisole) have been tried to see the effect of the halogen group. Cl-anisole gave the least conversion and selectivity to heterocoupled product (P1). On the other hand, I-anisole gave lower conversion than Br-anisole but the highest selectivity for product P1. This indicates that halogen with lower electronegativity gives high selectivity.

4.5 Conclusions

In this work we have shown that Au/ZrO_2 catalyst is best as compared to Au/TiO_2 and Au/Al_2O_3 in the oxidative coupling of bromoanisole with benzene. This is probably due to the redox nature of ZrO_2 support and small gold particle size. All the catalysts were synthesised by deposition-precipitation method. XPS for all the catalysts confirm the presence of gold in metallic state. The average particle size for Au/ZrO_2, Au/TiO_2, and Au/Al_2O_3 determined by TEM images is 4, 13.7, and 4.4 nm, respectively. Furthermore, the effect of different halogen group showed that the halogen with lowest electronegativity gives highest selectivity for heterocoupled product.

References

1. A. O. King, N. Yasuda in *Organometallics in Process Chemistry*, (Eds.: R. D. Larsen), Springer-Verlag, Berlin/Heidelberg, **2004**, pp. 205-246.
2. J. Corbet, G. Mignani, *Chem. Rev.*, **2006**, 106, 2651.
3. J. Hagen in *Industrial Catalysis*, Wiley-VCH, Weinheim, **2006**, pp. 59-80.
4. J. Hassan, M. Sévignon, C. Gozzi, E. Shulz, M. Lemaire, *Chem. Rev.*, **2002**, 102, 1359.
5. L. Gooßen, G. Deng, L. Levy, *Science*, **2006**, 313, 662.
6. S. Stanforth, *Tetrahedron*, **1998**, 54, 263.
7. L. Anastasia, E. Negishi, in Handbook of *Organopalladium Chemistry for Organic Synthesis*, (Eds.: E. Negishi), Ed. Wiley, New York, **2002**, pp. 311-334.
8. D. Alberico, M. Scott, M. Lautens, *Chem. Rev.*, **2007**, 107, 174-238; V. Ritleng, C. Sirlin, M. Pfeffer, *Chem. Rev.*, **2002**, 102, 1731.
9. J. Tsuji, H. Nagashima, *Tetrahedron*, **1984**, 40, 2699.
10. T. Matsumoto, H. Yoshida, *Chem. Lett.*, **2000**, 1064.
11. E. M. Beccalli, G. Broggini, M. Martinelli, S. Sottocornola, *Chem. Rev.*, **2007**, 107, 5318.
12. R. Scholl, C. Seer, Justus Liebigs, *Ann. Chem.*, **1912**, 111.
13. M. Takahashi, K. Masui, H. Sekiguchi, N. Kobayashi, A. Mori, M. Funahashi N. Tamaoki, *J. Am. Chem. Soc.* **2006**, 128, 10930.
14. S. Potavathri, A. Dumas, T. Dwight, G. Naumiec, J. Hammann, B. DeBoef, *Tetrahedron Lett.*, **2008**, 49, 4050.
15. D. Stuart, E. Villemure, K. Fagnou, *J. Am. Chem. Soc.*, **2007**, 129, 12072.
16. D. Stuart, K. Fagnou, *Science*, **2007**, 316, 1172.
17. G. Hutchings, *J. Catal.*, **1985**, 96, 292.
18. M. Haruta, N. Yamada, T. Kobayashi, S. Iijima, *J. Catal.*, **1989**, 115, 301.
19. A. Kar, N. Mangu, H. Kaiser, M. Tse, *J. Organomet. Chem.*, **2009**, 694, 524.
20. P. Serna, A. Corma, *ChemSusChem*, **2014**, 7, 2136.

Chapter 5. Bimetallic Gold Catalysts for Oxidation Reaction

5.1 Introduction

Supported bimetallic catalysts have gained lot of interest in the field of catalysis because they act as catalysts in many important reactions such as: NO reduction,[1] ethane hydrogenolysis,[2] methanol oxidation in so-called "direct methanol fuel cells",[3,4] olefin hydrogenation,[5,6] and conversion of cellulose to hexitols.[7] Apart from catalysis, bimetallic nanoparticles have also been used in technologically important areas like optoelectronic and magnetic.[8] There are two possible reasons for the interest in bimetallic nanoparticles: (i) they may show a difference in catalytic activity compared to their monometallic counterparts and (ii) it is possible to tune the chemical and physical properties of bimetallic nanoparticles by changing the composition. Various bimetallic nanoparticles have been studied for example, Ag–Au, Cu–Ag, Pd–Ag, Au-Co, Pt–Ag, Pd–Au, Pt–Au, Cu–Pd and Ni–Pt.[9-11] However, only Au-Pd combination has attracted much attention, since alloying of gold with some other metal has resulted in an increase of the catalytic activity and has significantly influenced the selectivity of the catalyst. Supported Au-Pd nanoalloys have been used in various reactions for example, direct synthesis of H_2O_2 from its elements,[12] hydrogenation of hex-2-yne to cis-hex-2-ene epoxidation of alkenes,[13,14] oxidation of alcohols, polyols,[15,16] and oxidation of toluene.[17] Nevertheless, styrene epoxidation and ethylbenzene oxidation have not been studied with supported Au-Pd nanoalloys.

Epoxidation of styrene is a commercially important reaction because it produces styrene oxide, an important organic intermediate in the synthesis of fine chemicals and pharmaceuticals. Very few bimetallic nanoalloys have been studied in styrene epoxidation. However, it has been observed that conversion is optimum but selectivity for styrene oxide is low. For instance Xinhong et al. have shown AuPt@SiO_2 hollow sub microsphere as the best catalyst with styrene conversion of 74% and styrene oxide selectivity of 85% after 12 h.[18] Very recently, Xiangcun

et al. have synthesised AuPt nanoalloy yolk@shell hollow particles and observed good catalytic performance for styrene epoxidation with the styrene conversion and styrene oxide selectivity of 85% and 87% in 12 h, respectively.[19] Both have shown that the unique mesoporous hollow spherical structure as well as presence of platinum is responsible for the activity of the catalyst. But there are no reports with Au-Pd nanoalloy catalyst.

Ethylbenzene oxidation is important because it produces acetophenone, which is used as a component of perfumes and as an intermediate for the manufacture of pharmaceuticals, resins, alcohols, and aldehydes.[20] Earlier, acetophenone was synthesised by using oxidants such as $KMnO_4$ or $K_2Cr_2O_7$ or Friedel−Crafts acylation employing acid halides or acid anhydrides as reagents and $AlCl_3$ as catalyst.[20] Presently, oxidants such as H_2O_2 and O_2 are used as an oxidant but this needs preparation of highly active and selective, O_2-activating heterogeneous catalysts.[21]

5.2 Synthesis of mono- and bimetallic catalysts

Bimetallic catalysts were prepared by the sol-immobilisation method, described in **Chapter 1**. The nominal metal loading in case of the bimetallic catalyst was fixed to 1 wt.% for each metal and in the monometallic the metal loading was fixed to 2 wt.%. The gold and palladium precursors are, $HAuCl_4 \cdot xH_2O$ and $PdCl_2$ were used in preparation. Stabiliser PVA (Polyvinyl alcohol) and carrier TiO_2 were used as received. Hereafter, bimetallic Au-Pd catalyst and its monometallic counterparts will be denoted as Au-Pd/TiO_2, Au/TiO_2, Pd/TiO_2.

5.3 Catalysts characterisation

To study the structural and textural properties, all the catalysts were characterised with different characterisation techniques such as XRF, powder X-ray diffraction, N_2 sorption, XPS, and TEM.

XRF confirms the successful loading of metals on support. The surface area (S_{BET}) of the supported catalyst is similar to the carrier which indicates that metals are deposited on the surface of the support. The powder X-ray diffractograms show no reflections due to Au and Pd which could be due to the very low loading of metal and presence of tiny metal particles (<5 nm) on the support.

Average particle size calculated for Pd/TiO_2, Au/TiO_2, and $Au\text{-}Pd/TiO_2$, from either STEM-HAADF or HRTEM image shows particle size of 2.3, 2.2, and 2.3 nm. This result clearly support the second conclusion (presence of tiny metal particles on support) obtained from the analysis of XRD patterns. To know the nature of Au and Pd distribution in the bimetallic system areas in HAADF-STEM image of $Au\text{-}Pd/TiO_2$ were subjected to elemental mapping and thus, confirms the formation of a nanoalloy.

Surface sensitive XPS study was done to know the nature of Au and Pd, and the interaction between Au and Pd in bimetallic system. In the monometallic catalyst the binding energy of Au 4*f* and Pd 3*d* indicates the presence of Au(0) and Pd(0). However, these binding energies are slightly shifted to lower binding energy which could be due to the strong interactions between Au and Pd that leads to the change in electronic properties of both Au and Pd, which again confirms the formation of the alloy nanostructures.[22,23] However, the shift is not towards higher binding energies which means that Au and Pd do not form any ionic species and maintain their metallic nature also in their alloy.

5.4 Catalytic activity in styrene and ethylbenzene oxidation

The oxidation of styrene to styrene oxide was investigated with $Au\text{-}Pd/TiO_2$, Au/TiO_2, and Pd/TiO_2 at 80°C using TBHP as an oxidant and acetonitrile as a solvent (**Figure 5.1**). No activity was observed without catalyst and with support only signifying the importance of catalyst in styrene epoxidation. Three different products were obtained namely: styrene oxide (SO) the desired one, acetophenone (ACP) (not obtained with Au/TiO_2), and benzaldehyde (BZ). The overall performance can be ranked as follows: $Au\text{-}Pd/TiO_2 > Au/TiO_2 > Pd/TiO_2$.

To explain the eminent behaviour of the $Au\text{-}Pd/TiO_2$ catalyst different characterisation parameters were considered. Metal loading, surface area, and particle size are similar in all the catalysts and therefore, it cannot explain the difference in performance. This undoubtedly guides us to conclude that it is due to the interaction present between Au and Pd in their nanoalloy form. The performance of the best catalyst ($Au\text{-}Pd/TiO_2$) was further optimised by varying the reaction parameters such as temperature, time, solvent, oxidant, and TBHP:styrene ratio. Increase in temperature till 80°C increases the conversion. As time increases the conversion increases steadily and reaches to 100% and 99% selectivity to styrene oxide which is the best selectivity obtained so far.

Acetonitrile and TBHP are the best solvent and oxidant. There is no marked difference with different TBHP:styrene ratios.

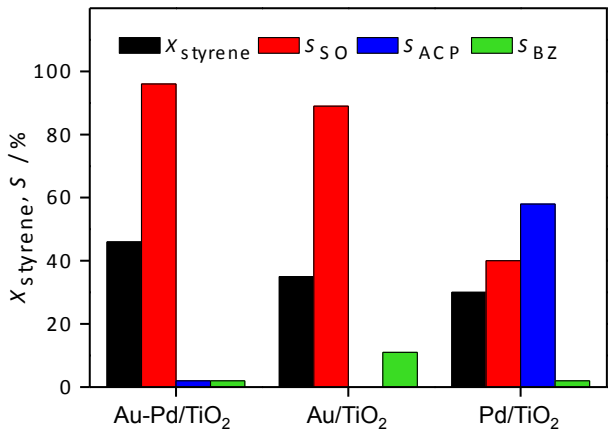

Figure 5.1 Styrene conversion and selectivity to products in styrene oxidation over the catalysts. Conditions: Catalyst = 0.06 g, T = 80°C, t = 6 h, TBHP:styrene = 1.6, and solvent = acetonitrile. $X_{styrene}$ = styrene conversion, S_{SO} = selectivity to styrene oxide, S_{ACP} = selectivity to acetophenone, S_{BZ} = selectivity to benzaldehyde.

The catalytic activities of Au-Pd/TiO_2, Au/TiO_2, and Pd/TiO_2 were also tested in ethylbenzene oxidation at 80°C for 24 h, with TBHP, acetonitrile as oxidant and

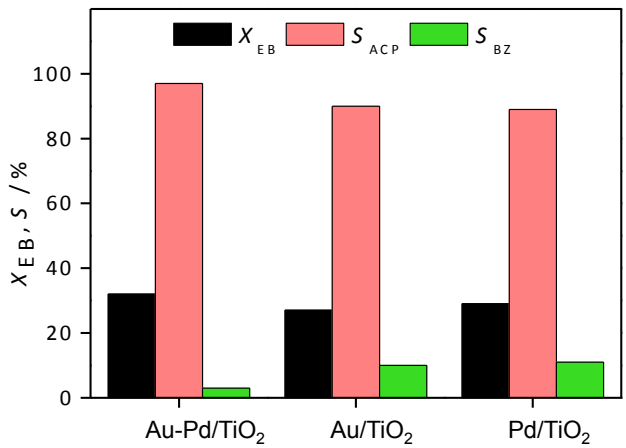

Figure 5.2 Ethylbenzene conversion and selectivity to products in ethylbenzene oxidation over the catalysts. Conditions: Catalyst = 0.06 g, T = 80°C, t = 24 h, TBHP:styrene = 1, and solvent = acetonitrile. X_{EB} = ethylbenzene conversion, S_{ACP} = selectivity to acetophenone, S_{BZ} = selectivity to benzaldehyde.

solvent, the results are displayed in **Figure 5.2**. Two products are obtained, acetophenone the major one and benzaldehyde as a side product. This reaction also shows that the bimetallic catalyst i.e Au-Pd/TiO_2 is best as compared to the monometallic systems.

5.5 Conclusions

This study demonstrates the synthesis of TiO_2 supported Au-Pd bimetallic and its monometallic counterparts by sol-immobilisation method. The catalytic activity of all the catalysts was evaluated in styrene epoxidation. XRF, TEM and surface area concluded the successful deposition of metal on carrier. Particles in all the catalysts are <5 nm as confirmed by TEM images. In both monometallic and bimetallic catalysts XPS showed the formation of Au(0) and Pd(0) species on the catalyst. Catalytic activity in styrene epoxidation identified Au-Pd/TiO_2 to be the best system with high conversion and highest selectivity. Optimisation of reaction parameters revealed that styrene conversion increases as temperature increases till 80°C after which it drops. Similarly, as time increases the conversion increases and reaches to 100% at 12 h with 99% of selectivity for styrene oxide, which is the highest selectivity, obtained so far. Among solvents and oxidants, acetonitrile and TBHP shows a positive effect on activity. However, the TBHP:styrene ratio has no prominent effect. In ethylbenzene oxidation again Au-Pd/TiO_2 has shown the best performance.

References

1. S. H. Zhou, B. Varughese, B. Eichhorn, G. Jackson, K. McIlwrath, *Angew. Chem., Int. Ed.*, **2005**, 44, 4539.
2. M. S. Nashner, D. M. Somerville, P. D. Lane, D. L. Adler, J. R. Shapley, R. G. Nuzzo, *J. Am. Chem. Soc.*, **1996**, 118, 12964.
3. C. Burda, X. B. Chen, R. Narayanan, M. A. El-Sayed, *Chem. Rev.*, **2005**, 105, 1025.
4. S. Wasmus, A. Ku¨ver, *J. Electroanal. Chem.*, **1999**, 461, 14.
5. N. Toshima, M. Harada, T. Yonezawa, T. Kushihashi, K. Kushihashi, K. Asakura, *J. Phys. Chem.*, **1991**, 95, 7448.
6. N. Toshima, T. Yonezawa, K. Kushiashi, *J. Chem. Soc., Faraday Trans.*, **1993**, 89, 2537.
7. J. Pang, A. Wang, M. Zheng, Y. Zhang, Y. Huang, X. Chen and T. Zhang, *Green Chem.*, **2012**, 14, 614.
8. G. Schmid, A. Lehnert, J. O. Malm, J. O. Bovin, *Angew. Chem., Int. Ed. Engl.*, **1991**, 30, 874.
9. M. Mirdamadi-Esfahani, M. Mostafavi, B. Keita, L. Nadjo, P. Kooyman and H. Remita, *Gold Bull.*, **2010**, 43, 49.
10. C. M. Doudna, M. F. Bertino and A. T. Tokuhiro, *Langmuir*, **2002**, 18, 2434.
11. C. M. Doudna, M. F. Bertino, F. D. Blum, A. T. Tokuhiro, D. Lahiri-Dey, S. Chattopadhyay, J. Terry, *J. Phys. Chem. B*, **2003**, 107, 2966.
12. J. K. Edwards, B. Solsona, E. Ntainjua N, A. F. Carley, A. A. Herzing, C. J. Kiely, G. J. Hutchings, *Science*, **2009**, 323, 1037.
13. M. D. Hughes, Y. J. Xu, P. Jenkins, P. McMorn, P. Landon, D. I. Enache, A. F. Carley, G. A. Attard, G. J. Hutchings, F. King, E. H. Stitt, P. Johnston, K. Griffin, C. J. Kiely, *Nature*, **2005**, 437, 1132.
14. J. Huang, T. Akita, J. Faye, T. Fujitani, T. Takei, M. Haruta, *Angew.Chem., Int. Ed.*, **2009**, 48, 7862.
15. D. I. Enache, J. Edwards, P. Landon, B. Solsana-Espriu, A. F. Carley, A. Herzing, M. Watanabe, C. J. Kiely, D. W. Knight, G. J. Hutchings, *Science*, **2006**, 311, 362.

16. L. Prati and M. Rossi, *J. Catal.*, **1998**, 176, 552.
17. L. Kesavan, R. Tiruvalam, M. I. Bin Saiman, D. I. Enache, R. Jenkins, N. Dimitratos, J. A. Lopez-Sanchez, S. H. Taylor, D. W. Knight, C. J. Kiely, G. J. Hutchings, *Science*, **2011**, 351, 195.
18. X. Qi, X. Li, G. He, Y. Zhu, Y. Diao, H. Lu, *Chemical Engineering Journal*, **2016**, 284, 351.
19. X. Li, W. Zheng, B. Chen, L. Wang, G. He, *ACS Sustainable Chem. Eng.*, **2016**, 4, 2780.
20. R. Alcántara, L. Canoira, P. G. Joao, J. M. Santos, I. Vázquez, *Appl. Catal. A: Gen.*, **2000**, 203, 259; H. J. Sanders, H. F. Keag, H. S. McCulloug, *Ind. Eng. Chem.*, **1953**, 45, 2.
21. K. O. Xavier, J. Chako, K. K. M. Yusuff, *Appl. Catal. A: Gen.*, **2004**, 258, 251.
22. H. Chen, J. Huang, D. Huang, D. Sun, M. Shao, Q. Liabd, *J. Mater. Chem. A*, **2015**, 3, 4846.
23. J. Chai, F. H. Li, Y. Hu, Q. X. Zhang, D. X. Han, L. Niu, *J. Mater. Chem.*, **2011**, 21, 17922.

Sheetal Sisodiya was born on 14th December in Pune, India. She has done her Master studies in Organic Chemistry from University of Pune in 2007. After finishing her master studies she joined National Chemical Laboratory, Pune, India as a project assistant; where she was involved in several projects with main emphasis on the development of polysiloxane catalyst, metal incorporated mesoporous materials, and transition metal complex supported on periodic mesoporous organosilica for oxidation reactions. In August 2011 she joined as a PhD student in Prof. Ola F. Wendt's research group at Centre for Analysis and Synthesis (CAS), Department of Chemistry, Lund University, Sweden. During her PhD studies she has worked on supported gold mono- and bimetallic catalysts for different coupling and oxidation reaction.

Printed by Media-Tryck, Lund 2017 NORDIC ECOLABEL, 3041 0903

LUND UNIVERSITY

ISBN 978-91-7422-533-4 (print)
ISBN 978-91-7422-534-1 (pdf)

Centre for Analysis and Synthesis
Department of Chemistry
Faculty of Science
Lund University